

1 **Oblique rifting triggered by slab tearing : the case of the Alboran**
2 **rifted margin in the eastern Betics**

Deleted: and back-arc extension

Deleted: rift

3
4 Marine Larrey^{1,2}, Frédéric Mouthereau^{1*}, Damien Do Couto³, Emmanuel Masini⁴, Anthony
5 Jourdon⁵, Sylvain Calassou² and Véronique Mieggebielle²

6 ¹Université Paul Sabatier, Géosciences Environnement Toulouse, GET UMR 5563, Toulouse, France.

7 ²TOTAL S.A., Centre Scientifique & Technique Jean Féger, Pau, France.

8 ³Sorbonne Université, CNRS-INSU, Institut des Sciences de la Terre Paris, ITeP UMR 7193, F-75005 Paris,
9 France.

10 ⁴M&U sas, France.

11 ⁵Institute of Geophysics, Ludwig-Maximilians-Universität München, Munich, Germany.

12 *Corresponding author:* Frédéric Mouthereau (frederic.mouthereau@get.omp.eu)

13
14 **Abstract**

15 The tectonic evolution of highly oblique continental margins that result from back-arc extension above lithospheric
16 STEP faults is poorly understood. Here, we investigate the case of the Alboran margin in the eastern Betics
17 characterized by crustal thinning of 15-10 km, oblique to the direction of slab retreat. The current deformation patterns
18 indicate that oblique back-arc rifting is underway. However, it is unclear whether these conditions are those that
19 prevailed during the formation of the metamorphic domes and intramontane basins. We review the temporal and
20 spatial evolution of Neogene sedimentary basins and brittle deformation in the eastern Betics, and exploit offshore
21 seismic reflection lines to propose a crustal-scale section across the oblique margin. The history of sediment infill and
22 rates of subsidence combined with the analyses of fault slip data, confirms that brittle extension oriented from N20°E
23 to EW occurred during an interval spanning from the Serravallian-early Tortonian to the late Tortonian (14-8 Ma).

Deleted: confirm

24 This extension is associated with both normal and strike-slip regimes and the evolution of the strike-slip fault zones
25 flanking the metamorphic domes. The transtensional model forms a coherent scheme linking the ductile deformation
26 associated with metamorphic domes and the formation of EW- and NW-SE/NNW-SSE-directed sedimentary basins
27 in the brittle upper crust during the Tortonian. The oblique extension, which is closely associated with STEP faulting,
28 occurred during the regional convergence between Africa and Iberia since the Miocene. Only recently, around 8 Ma,
29 slab detachment started to migrate westward, leading to tectonic inversion in the eastern Betics. Such a type of narrow
30 oblique rifted margin associated with transform-like plate boundaries is not unique but is expected to be hardly
31 preserved in the geological record due to the transient nature of retreating subduction systems.

Deleted: found

Deleted: corridors

Deleted: the

Deleted: detached

Deleted: local

40 **1 Tear faulting and the formation of oblique, rifted margin in the Betics**

41 Lithospheric tear faults or subduction-transform edge propagator (STEP) faults are propagating strike-slip faults that
42 accommodate the differential motion between the retreating subduction zone and the overriding back-arc plate (Govers
43 and Wortel, 2005). Because of the relative motion between back-arc and surrounding plates, they are also propagating
44 strike-slip faults defined by a sharp contrast in crustal thickness. As noted by Govers and Wortel (2005) such oblique
45 fault boundaries do not necessarily form proper transform plate boundaries but broad zones of distributed deformation,
46 accommodating differential trench-parallel extension, strike-slip motion and rotation. In case the lithospheric tear
47 propagates within the continent-ocean transition, a narrow continental margin forms highly oblique to the direction of
48 back-arc extension. This is documented, for instance, in the Carribean, along the transcurrent Carribean-South
49 America plate boundary (Pindell and Kennan, 2009) or on the margin of the South Orckney microcontinent, along the
50 Scotia-Antarctic plate boundary (Dalziel et al., 2013). Despite the large-scale kinematic picture is relatively well
51 understood, there are only few places on Earth where continental crustal deformation associated with slab-edge
52 continental rift system can be studied both onland and offshore.

53 Here, we focus on the eastern Betic Cordillera, which constitutes a rifted margin, defined by decreasing crustal
54 thickness from >35 km to 20 km (Diaz et al., 2016) (Figs 1 and 2). This region is seen to develop above a STEP fault
55 at the boundary between the Alboran basin and the Iberian paleomargin (Badji et al., 2014; Gallais et al., 2013; Jolivet
56 et al., 2021a; Mancilla et al., 2015a). The tectonic expression of the transcurrent deformation during crustal extension
57 above the lithospheric tear is however controversial. On the one hand, low-angle ductile extensional detachments with
58 a top-to-the-west sense of shear are the main features accommodating deformation in the overriding plate. Yet, a-type
59 metamorphic domes in the lower crust, elongated parallel to the E-W direction (Fig. 1), are viewed to express the
60 transtensional deformation at the tip of propagating tear (Pourhiet et al., 2012). On the other hand, strike-slip faulting
61 is interpreted as a late brittle deformation feature associated with differential E-W crustal extension between the
62 metamorphic domes in the eastern Betics (Alpujarras fault zone; Sanz de Galdeano and Vera, 1992; Sanz de Galdeano
63 et al., 1985; Martínez-Martínez et al., 2006) and in the western Betics (e.g. Torcal fault zone; Frasca et al., 2016 ;)
64 unrelated to ductile deformation (Fig. 1). In line with the latter interpretation, the dextral motion these strike-slip
65 transfer faults accommodate is assumed to be modest, reflecting a recent post-8 Ma kinematic change that accompanies
66 the stalling of westward slab rollback, the onset of tectonic inversion in the Gibraltar Arc (Do Couto et al., 2014;
67 d'Acremont et al., 2020; Jolivet et al., 2021a; Martínez-García et al., 2017), and progressive slab tearing and
68 delamination of the lithospheric mantle from the eastern to the central Betics (Mancilla et al., 2015a; García-
69 Castellanos and Villaseñor, 2011; Spakman et al., 2018).

70 The lack of structural, temporal constraints and quantification of belt-parallel motion along these faults indicates,
71 however, that we do not yet fully understand their link with the long-term evolution of slab tearing _____ and
72 margin formation. For instance, the current deformation patterns in the Central Betics, where metamorphic domes are
73 present, brings evidence that both strike-slip faulting and extension operate synchronously. This is shown by the west-
74 directed GPS velocities increasing westwards indicating ongoing extension, and the west-directed displacements
75 increasing from North to South, towards the Alboran domain, revealing right-lateral shear, (Fig. 2). The current
76 transtensional deformation across the Betic Cordillera is consistent with the current stress regime defined by extension

Deleted: transform

Deleted: this peculiar type of

Deleted: on the northern boundary of the Gibraltar arc (Figs 1 and 2). There,

Deleted: ,

Deleted: in the Alboran basin

Deleted:),

Deleted: strike-slip brittle faults

Deleted: corridor

Deleted: corridor

Deleted: end

Deleted: retreat, and

Deleted: compression

Deleted:).

Formatted: Font colour: Black

Deleted: critical

Deleted: , so that brittle strike-slip faulting and ductile extension might reflect the same tectonic episode.

Deleted: argued by ongoing extension illustrated by

Deleted: active

Formatted: English (US)

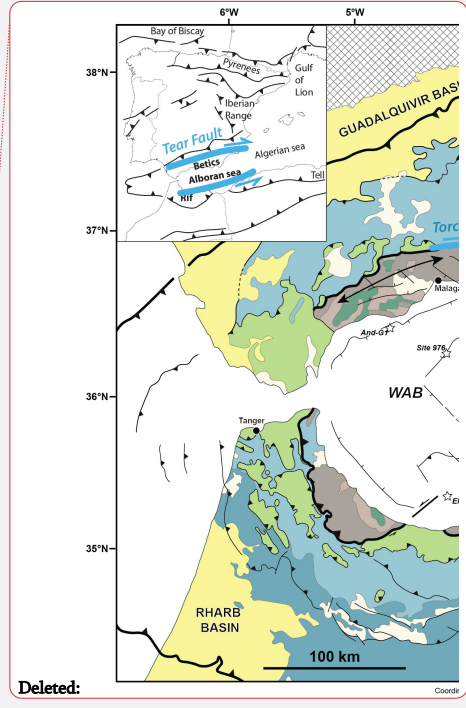
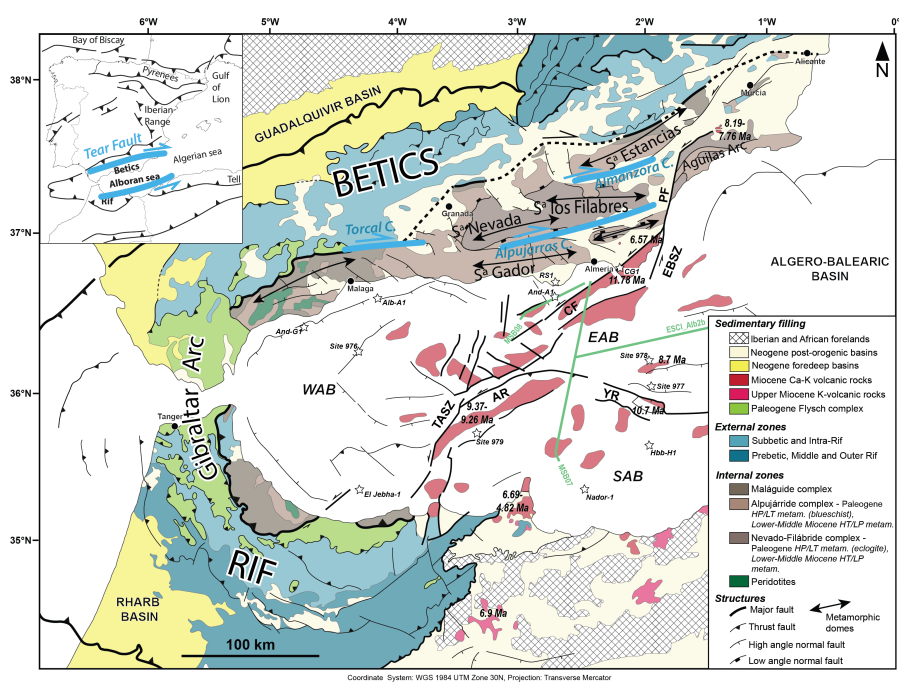
Deleted: deformation

Formatted

Deleted: also shown by

98 direction highly oblique (max. 20°) to the Betic structural trend (or 70° spanned by the direction of extension and
 99 normal of the rift trend). Right-lateral transtensional deformation further agrees with the extrusion model of the
 100 Alboran basin towards the Gibraltar arc to the West (Borque et al., 2019; Palano et al., 2015) as a consequence of
 101 indentation by the east Abloran domain likely enhanced by resistance slab dragging (Spakman et al., 2018). In the
 102 East, the extrusion is accommodated by left-lateral strike-slip displacement along the Eastern Betic Shear Zone
 103 (EBSZ; Borque et al., 2019), shaped by the Carboneras Fault (CF) and Palomares Fault (PF), which separates the
 104 extrusion domain where extension and transtension is prevailing from the Águilas Arc where N-S indentation is well
 105 documented (Ercilla et al., 2022). This fault extends offshore, across the Alboran Sea, in the larger Trans-Alboran
 106 Shear Zone (De Larouzière et al., 1988; Stich et al., 2006) moving at ~4 mm/yr, equivalent to the regional 5 mm/yr
 107 NW-directed convergence between Africa (Nubia) and Europe (Fig. 2; Echeverría et al., 2013; Kouli et al., 2011;
 108 Nocquet, 2012; Palano et al., 2015, 2013; Vernant et al., 2010). Here, we hypothesize that the present-day oblique
 109 extension patterns is at play since the Miocene and explain the formation of the narrow Alboran rifted margin.

- Deleted: in the Betic
- Deleted: evidence for west-directed lateral
- Formatted: English (US)
- Deleted: Basin
- Deleted:).
- Deleted: east
- Deleted: which is
- Deleted: Palomeras
- Formatted: English (US)



120 **Figure 1** : Geological map of the Betic-Rif arc. Main tectonic units and age of volcanism as well as major structures and Neogene sedimentary basins are shown. The studied offshore seismic lines (red) is displayed as well as offshore wells and ODP sites (★) for stratigraphic calibration in the East (EAB), South (SAB) and West Alboran basins (WAB). CF: Carboneras Fault; PF : ~~Palomares~~ Palomares Fault; AR: Alboran Ridge; YR: Yusuf Ridge; EBSZ : East Betic Shear Zone; TASZ: Trans-Alboran Shear Zone.

126 Only recently high-resolution 3D numerical models have been able to predict the deep structure of oblique rift domains. These models can be used as a guide to re-evaluate the evolution of the ~~Betics~~ Betic region. 3D models by Jourdon et al. (2021) predict that oblique extension results in narrow rifted margins, strike-slip faults and corridors coupled with subsident pull-apart basins, normal faults and block rotations (Fig. 3). The recognition of block rotation in the Betic arc (Crespo-Blanc et al., 2016; Platzman, 1992), strike-slip ~~fault zones~~ fault zones (Fig. 1) and NW-SE normal faulting, which defines extension direction highly oblique to the margin, (Galindo-Zaldivar et al., 2003; Figs 1 and 2), support this view. The simulations also show that the deeper ductile crust experiences thinning (vertical flattening) and stretching perpendicular to the strike of the margin in accordance with stretching lineations parallel to the metamorphic domes and low-angle detachments (Fig. 3). Other types of 3D numerical experiments show that sediment loading of strike-slip faults can result in asymmetric flexural basin with apparent normal fault throw (Neuharth et al., 2021) that can be mistakenly interpreted as resulting from orthogonal extension. Asymmetric basins are indeed intriguing characteristics of intramontane basins in the Betics (Rodríguez-Fernández et al., 2011; Augier et al., 2013; Do Couto et al., 2014; Giaconia et al., 2014). Although primarily found associated with divergent plate boundaries e.g. in the Gulf of California (Fossen et al., 2013; Fossen and Tikoff, 1998) highly oblique extension is also documented in active transform regions along the San Andreas Fault (Teyssier and Tikoff, 1998) or the North Anatolian Fault in Marmara Sea (Okay et al., 2004). A detailed analysis of highly oblique rifting deformation in the Gulf of California recognises similar tectonic elements as for the Betics, such as extensional detachment systems orthogonal to the divergence and upper crustal folds trending parallel to the divergence (Fossen et al., 2013).

~~Deleted:~~ Palomeras

~~Deleted:~~ Betic region

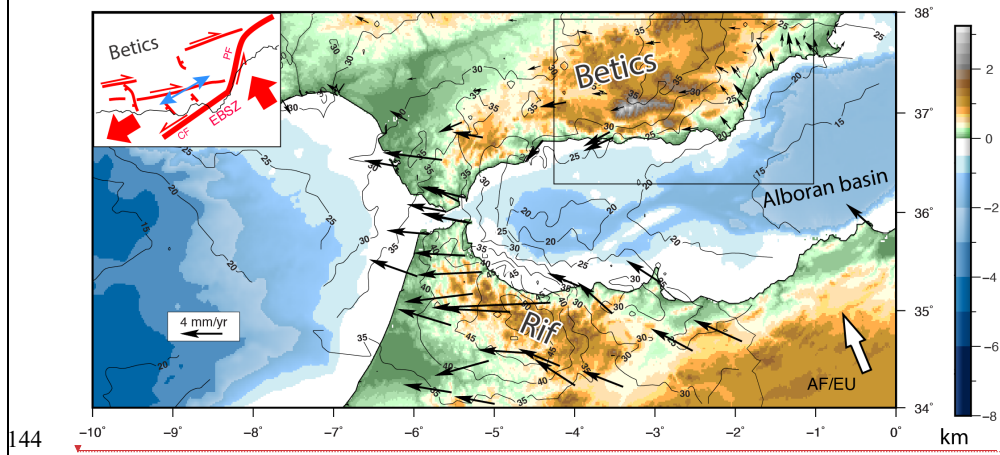
~~Deleted:~~ corridors

~~Deleted:~~ ,

~~Deleted:~~) all

~~Deleted:~~ of Jourdon et al. (2021)

Formatted: English (US)



Formatted

~~Deleted:~~ ¶

144 **Figure 2** : Present-day kinematics in the Betic-Rif arc and eastern Betic Cordillera (inset). GNSS-based displacements in the ~~western Alboran~~ western Alboran block and ~~north-western~~ north-western Africa shown in a fixed Eurasian reference frame (black arrows after

~~Deleted:~~ Abloran

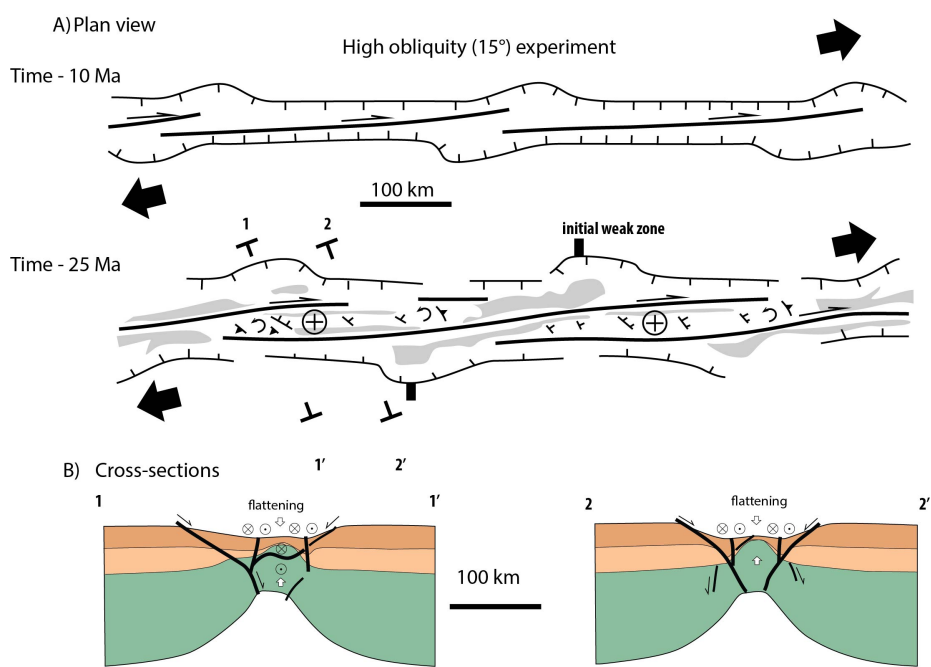
~~Deleted:~~ northern

157 Palano et al., 2015) are oblique to the AF/EU plate convergence (white arrow) inferred from plate tectonic Morvel
 158 model (Argus et al., 2011). Labelled contours depict the crustal depth given in kilometers as inferred from deep seismic
 159 profiles and receiver functions analysis (Diaz et al., 2016). In the eastern Betic (inset), W-directed stretching is taken
 160 up by EW-directed right-lateral strike-slip fault and NW-SE normal faults. Extension direction resolved from focal
 161 mechanisms (blue arrows) are after (Stich et al., 2006). CF: Carboneras Fault; PF : Palomares Fault; AR: Alboran
 162 Ridge; YR: Yusuf Ridge; EBSZ : East Betic Shear Zone; TASZ: Trans-Alboran Shear Zone.

Deleted: Palomeras

164 Several tectonic features need further discussion however. First, the relevance of strike-slip faulting in the past is
 165 debatable as only a few occurrence of crustal-scale strike-slip faults are mapped. Second, the detail of the temporal
 166 and spatial relationships between the formation of the oblique/transform margin and STEP faulting remain elusive.
 167 We here review the temporal and spatial evolution of Neogene intramontane sedimentary basins and related brittle
 168 deformation in the eastern Betics. In addition, we exploit offshore seismic reflection lines to propose a new crustal-
 169 scale section across the oblique margin. Based on these constraints we present a tectonic scenario for the formation of
 170 the high-obliquity rifted margin controlled by STEP faulting.

Deleted: rift
 Deleted: in back-arc setting



172
 173 **Figure 3** : Sketch showing two steps (after 10 Myrs and 24 Myrs) of a 3D thermo-mechanical model of oblique rifting
 174 in plan view (A) and cross-sections (B). Results are redrawn after (Jourdon et al., 2021) for the case of a highly oblique
 175 experiment where extension is set with an angle of 15° with respect to the rift axis. Grey regions in (A) are basins
 176 adjacent to uplifted domains (cross-circle symbol) associated with right-lateral strike-slip faults. Cross-sections (B)
 177 depict the abrupt crustal thinning that occur perpendicular. Crustal thinning is most visible for the lower crust and
 178 produces the formation of an abrupt necking domain controlled by rift-parallel normal faults dipping towards the
 179 center of the rift and right-lateral strike-slip faults.

183

184 2. Geodynamics and STEP faulting in the Betics

185 The onset of N-directed movement of Africa, by the Late Cretaceous-Paleogene, led to ~~far-field~~, Laramide-like
186 contraction from Morocco throughout Western Europe (Mouthereau et al., 2021). South of Iberia, in the Betic-Rif
187 domain, the closure of hyper-extended rift systems and oceanic basins of the Atlantic-Alpine Tethys resulted in the
188 development of a proto-Betic accretionary prism, likely largely submerged (Angrand and Mouthereau, 2021; Daudet
189 et al., 2020; Vergés and Fernández, 2012). By about 50 Ma, the acceleration of plate convergence led to the shortening
190 of continental rift and oceanic basins and topographic uplift all over Iberia (Daudet et al., 2020; Mouthereau et al.,
191 2021, 2014; Rat et al., 2019; Vacherat et al., 2016; Waldner et al., 2021) associated with onset of continental rifting
192 along the Western European Rift (e.g. Mouthereau et al., 2021). 35 Ma ago, as Africa convergence slowed down, the
193 western Mediterranean sea opened accompanied by retreating slabs (Dewey, 1988; Dewey et al., 1989; Faccenna et
194 al., 2014; Jolivet and Faccenna, 2000; Rosenbaum et al., 2002). Subduction occurred mainly before 30 Ma as argued
195 by age constraints on high-pressure mineral assemblages (Augier et al., 2005a; Bessièrè et al., 2021; Booth-Rea et al.,
196 2015; Gomez-Pugnaire and Fernandez-Soler, 1987; Platt and Vissers, 1989; Platt and Whitehouse, 1999) and has been
197 suggested to last until the mid-Miocene in the eastern Betics e.g. (Platt et al., 2013). The timing of formation of the
198 Alboran basin is constrained to 23 to 16 Ma by the oldest deposits found on Alboran basement and by the timing of
199 high-temperature metamorphic overprint and rapid cooling to shallow crustal temperature (Bessièrè et al., 2021;
200 Daudet et al., 2020; Janowski et al., 2017; Johnson et al., 1997; Platt et al., 2005; Sosson et al., 1998; Vázquez et al.,
201 2011; Zeck et al., 1992). ~~The eastern Alboran basin formed later, mostly by late Miocene arc magmatism (Booth-Rea~~
202 ~~et al., 2007; 2018; Gómez de la Peña et al., 2020a).~~

203 All kinematic reconstructions agree that extension results from the westward migration of the arc front and retreat of
204 the Alboran slab, well imaged below the Gibraltar arc as a steeply-dipping high-velocity anomaly (Bezada et al., 2013;
205 Heit et al., 2017; Mancilla et al., 2018, 2015a, 2015b; Palomeras et al., 2014; Spakman and Wortel, 2004; Villaseñor
206 et al., 2015). These reconstructions, however, differ according to the paleo-position of Alboran terrane, and hence to
207 the amount and vergence of subduction (Angrand and Mouthereau, 2021; Hinsbergen et al., 2014; Lonergan and
208 White, 1997; Romagny et al., 2020; Rosenbaum et al., 2002; Vergés and Fernández, 2012). Seismic tomography
209 reveals that slab detachment and tearing occur along the conjugate Alboran margins of the southern Betics and
210 northern Africa (Govers and Wortel, 2005; Heit et al., 2017; Mancilla et al., 2015a; Meighan et al., 2013; Spakman
211 and Wortel, 2004).

212 In Fig. 4 we refer to the reconstruction of Angrand and Mouthereau (2021) that has the advantage of reconciling
213 previous western Mediterranean models (Romagny et al., 2020; Vergés & Fernández, 2012) with recent
214 thermochronological analyses in western Betics (Daudet et al., 2020) and other geological data (see compilation in
215 Mouthereau et al., 2021). ~~This model considers that the Alboran domain has been rifted from Iberia during the Jurassic.~~
216 ~~It is in agreement with detrital and igneous zircon U-Pb ages that suggest Alboran was attached to Iberia in the late~~
217 ~~Paleozoic (Jabaloy-Sánchez et al. 2021). It also~~ accounts for the existence of an upper Cretaceous-Paleogene foreland
218 basin that formed adjacent to a proto-Betic orogen, ~~and in continuity eastwards with the Balearic Promontory. In that~~

Deleted: a

Deleted: Romain

Formatted: English (US)

Deleted: This model

Deleted: .

respect, it contrasts with other models placing the Alboran domain to the south of the Balearic Promontory (Moragues et al., 2021; van Hinsbergen et al., 2014).

In this reconstruction about 400 km of slab retreat is estimated since about 35 Ma (gray path, blue arrows in Fig. 4). It is worth noting that for Romagny et al. (2020) a similar amount (i.e. 400 km) is accommodated by back-arc extension of the Alboran crust, implying the same magnitude of displacement along the STEP fault in the Betics. In the reconstruction of Angrand and Mouthereau (2021), however, crustal thinning in Alboran basin is linked to delamination ~~retreat~~ of the Alboran lithospheric mantle towards the west. ~~Because~~ of the decoupling between crust and mantle, the length of the delaminated slab resolved at depth in seismic tomography, should not be simply translated into the amount of E-W crustal extension in the Alboran domain. This further implies ~~that~~ the displacement across the STEP fault must be also less than 400 km. Daudet et al. (2020) suggested that an extension of 110 km estimated from the restoration of low-angle detachment systems in the central and eastern Betics (Martínez-Martínez et al., 2002) is likely to be a more accurate crustal estimate of the movement Alboran domain ~~rather~~ than the total slab length.

~~Deleted:~~ retrat

~~Deleted:~~ In such a model, because

~~Deleted:~~ ratchr

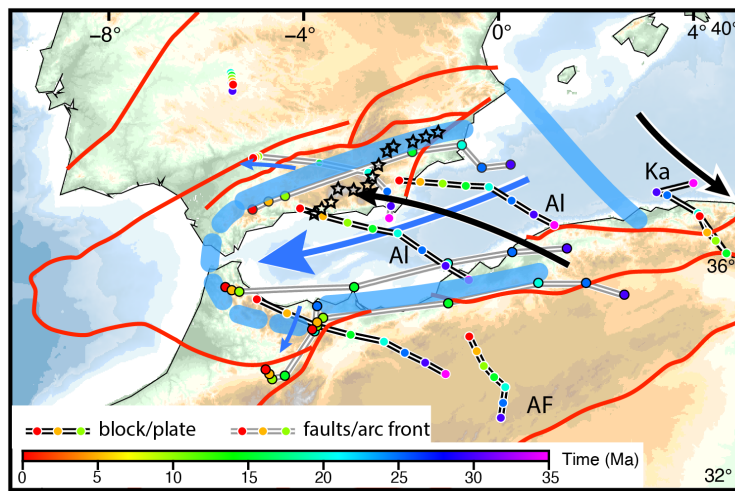


Figure 4: Kinematics of African plate (AF), Alboran (Al) and Kabylides (Ka) blocks with respect to fixed European plate since 35 Ma reconstructed after Angrand and Mouthereau (2021). Thick blue lines depicts the approximate position of lithospheric tear faults (between Al and Europe and Africa) and transfer faults (between Al and Ka). ~~Tear faults located in Betics and Rif are after Jolivet et al. (2021b). Black stars depicts the positioned of tear fault in the Betics as defined by Mancilla et al. (2015a). Black arrows indicate the movement of Al and Ka with respect to Europe along black motion paths presented from 35 Ma to present. Grey motion paths refer to the motion of specific structures relative to Europe, including the motion of the arc front (thick blue dashed line) and faults in red. Dark blue arrow depicts the movement of the arc front due to retreating delamination towards the west.~~

~~Deleted:~~

~~Deleted:~~ Black arrows indicate the regional

3. Miocene extension in the eastern Betics

3.1 Relationships between domes and basins : from transtension and pure extension to late tectonic inversion

253 The most prominent extensional features in the eastern Betics are : 1) E-W elongated ranges that formed metamorphic
254 domes with foliations bearing prominent E-W stretching lineations, for instance, in the Nevado-Filabrides
255 Complex (Fig. 5; e.g. Sierra de los Filabres, Sierra Nevada, and the Sierra de las Estancias) and Serravallian-Tortonian
256 sedimentary basins (Tabernas-Sorbas, Alpujarras, Almanzora and Huércal-Overa basins); 2) NNW-SSE/NW-SE
257 normal fault systems and basins oblique to the domes such as the NW-SE trending Guadix-Baza and Alhabia basins
258 (Galindo-Zaldivar et al., 2003; Martínez-Martínez and Azañón, 1997) (Fig. 5). They are described as asymmetric half
259 grabens (Do Couto et al., 2014; Martínez-Martos et al., 2017; Pedrera et al., 2010, 2009) formed during the Upper
260 Serravallian-Early Tortonian (Augier et al., 2005b; Augier et al., 2013; Meijninger and Vissers, 2006). Several of
261 these NW-SE faults are active and cut across the metamorphic domes and the sedimentary basins (Augier et al., 2005a;
262 Booth-Rea et al., 2004; Giaconia et al., 2012; Montenat and Ott d'Estevou, 1999).

263 In addition to these structures, there are E-W right-lateral strike-slip fault zones and parallel depressions, like the
264 Alpujarras fault zone between the Sierra de Gádor and the Sierra Nevada, and the Almanzora fault zone between the
265 Sierra de los Filabres and Sierra de las Estancias (Fig. 5). The left-lateral Carboneras and Palomares fault system
266 (Reicherter and Hübscher, 2006; Scotney et al., 2000) marks the tectonic limit with the Cabo de Gata volcanic province
267 (Fig. 5).

268 The domes are extension-related features interpreted either as 1) EW-metamorphic domes resulting from the
269 exhumation in the footwall of a regional W-directed extensional low-angle detachments, later folded during post-
270 Tortonian N-S contraction (e.g. Montenat & Ott d'Estevou, 1990; Sanz de Galdeano and Vera, 1992; Sanz de
271 Galdeano and Alfaro, 2004; Martínez-Martínez et al., 2002; Martínez-Martos et al., 2017; Pedrera et al., 2010, 2007)
272 or 2) Miocene metamorphic domes formed by constrictional ductile strain regime accompanying W-directed
273 stretching of the Alboran domain and trench retreat, with limited overprint by the Tortonian contraction ca. 8 Ma
274 (Augier et al., 2013; Augier et al., 2005; Augier et al., 2005b; Galindo-Zaldivar et al., 2015; Jolivet et al., 2021b;
275 Martínez-Martínez et al., 2002). Low-temperature constraints from the Nevado-Filabride and Alpujarride complexes
276 confirm the west-directed exhumation of the basement that occurred progressively from the Sierra de los Filabres at
277 ~13-11 Ma (Serravallian) in the East to the Sierra Nevada at 8-6 Ma (Tortonian) in the West (Clark and Dempster,
278 2009; Janowski et al., 2017; Johnson et al., 1997; Platt et al., 2005; Reinhardt et al., 2007; Vázquez et al., 2011).

279

Deleted: -

Deleted: Sierra de Gador

Deleted: faults that define structural corridors

Deleted: corridor/basin

Deleted: corridor/basin

Deleted: Palomeras

Deleted: (

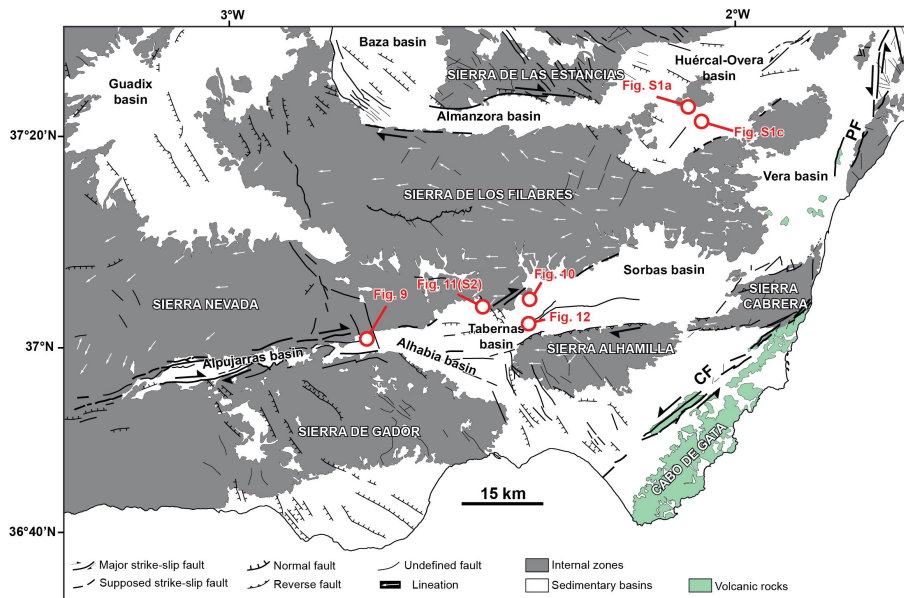


Figure 5 : Tectonic map of the eastern Betics showing the main structural elements in black after Augier et al. (2005) and Do Couto (2014). CF: Carboneras Fault; PF : Palomares Fault.

Tectonic models for the formation of Neogene intramontane sedimentary basins vary depending on the prevailing tectonic regime. EW-directed basins have been early described as pull-apart basins (e.g Alpujarran fault zone; Sanz de Galdeano et al., 1985). Structural analyses then led to re-interpret these structures as transfer zones resulting from differential extension between exhuming core-complexes (and detachment systems) since the Serravallian (13-11 Ma) later refolded during Tortonian (9-8 Ma) compression in the Eastern Betics while extension is still active in the Central Betics (Martínez-Martínez et al., 2006). Other authors proposed that NE-SW extension lasted until 7.5-7 Ma in the Eastern Betics (Booth-Rea et al., 2004; Giaconia et al., 2014).

In support to the compressional stress regime, in the Eastern Betics, Martínez-Martos et al. (2017) interpreted the E-W depressions are related to the tectonic reactivation of crustal weakness zone as dextral strike-slip faults in a counterclockwise rotation, accommodating part of the the N-S shortening. There are evidence that at the end of the Tortonian a regional uplift occurred, rising the remnants of late Tortonian marine platform, 7.2 Ma in age, to 1600 m above sea level in the Sierra de Gádor (Braga et al., 2003; Janowski et al., 2017), coincidentally with the onset of contraction in the Sierra Alhamilla and Sierra de los Filabres (e.g. Do Couto et al., 2014), in the Alboran domain (e.g. Martínez-García et al., 2017) and on the margins of the eastern Betic (Giaconia et al., 2013). In addition to shortening, this recent uplift may reflect deep mantle mechanisms like slab tearing or delamination (e.g. Duggen et al., 2003; García-Castellanos and Villaseñor, 2011; Mancilla et al., 2015a).

Deleted: Palomeras

Deleted: corridor) (

Deleted: dominant regional

Deleted: ,

Deleted: proposed

Formatted: English (US)

Deleted: (

Formatted: English (UK)

314 Based on the prevalence in some EW-trending basins, like the Huércal-Overa basin, of EW-trending normal faults,
315 these basins have alternatively been interpreted as resulting from late exhumation stage of the domes, possibly as soon
316 as the Serravallian, but mostly after the early Tortonian (syn-sedimentary faulting) (Augier et al., 2013; Augier et al.,
317 2005b; Meijninger and Vissers, 2006). The NW-SE/NNW-SSE sedimentary basins (Guadix, Baza, Alhabia; Fig. 5),
318 in contrast, are extensional basins formed parallel to the direction of the regional compression (Sanz de Galdeano and
319 Vera, 1992; Larouzière et al., 1988). E-W strike-slip fault zones, aligned in the direction of the domes, and NW-SE
320 normal faulting patterns are both key features consistent with predictions from models of oblique extension at
321 transform margin (Fig. 3). Yet, based on existing structural and tectonic syntheses a clear temporal relationships
322 between E-W ductile stretching in the domes and transcurrent deformation is not established (Fig. 5).
323

3.2 Is the Tortonian rift-related subsidence consistent with oblique extension ?

325 The stratigraphic architecture and depositional evolution of Tortonian intramontane basins provides first-order
326 informations on the distribution of crustal thinning. Among the oldest sediments deposited unconformably on the
327 Paleozoic-Triassic basement are the red alluvial conglomerates and deltaic series dated from the Serravallian to the
328 Lower Tortonian (Fig. 6a). They are thicker and well exposed on the flanks of the Almanzora basin and on the northern
329 Huércal-Overa basin (HOB), compared to the Alpujarras Corridor (AC) and Tabernas basin (TB) (Figs. 6 and 7a;
330 Augier et al., 2013; Pedrera et al., 2010, 2007; Poisson et al., 1996). East of Sorbas basin, it should be noted that
331 Langhian-Serravalian deposits and perhaps sediments as old as Burdigalian have been locally reported (Giaconia et
332 al., 2014).

333 Paleogeographic reconstructions indicate that these Serravallian to Lower Tortonian sediments were deposited on a
334 large emerged domain, stretching from Huercal-Overa to Granada, in the West and in Tabernas, to the South (Braga
335 et al., 2003). Sourced from the Nevado-Filabride metamorphic complex (Hodgson and Haughton, 2004; Kleverlaan,
336 1989; Meijninger and Vissers, 2006; Pedrera et al., 2010, 2007; Pickering et al., 2001; Weijermars et al., 1985) these
337 deposits mark the onset of surface exhumation of the Sierra de Las Estancias and Sierra de Los Filabres.

338 During this initial stage, HOB is the most subsident basin (Figs. 6b, 7a and 7b), accumulating sediments at rates of
339 400 m/Ma while rates are 140-180 m/Ma in the Tabernas basin (Fig. 6b) (Augier, 2005). Higher subsidence in the
340 HOB, which also started earlier than in other basins, suggests extension occurred originally to the North associated
341 with the exhumation of the Sierra de Las Estancias. Basal continental conglomerates are overlain by grey coarse-
342 grained Tortonian sandstones found occasionally, e.g. in the Almanzora basin, intercalated with marine marls (Figure
343 6a). They are topped by mid-Tortonian bioclastic calcarenite and coral reefs (Braga et al., 2003; Martin et al., 1989;
344 Pedrera et al., 2007).

345 During the same interval, TB recorded the deposition of 300 to 400 m of coarse to medium-grained deltaic marine
346 clastics overlying unconformably the lowermost red series (Fig. 6a). These sediments pass upwards, e.g. in TB, to
347 deeper marine 1200 m-thick turbiditic and marls series intercalated with regional-scale megabeds, revealing the onset
348 of rapid tectonic subsidence (Haughton, 1994; Kleverlaan, 1989, 1987; Pickering et al., 2001; Weijermars et al., 1985).

349 Details of depositional architecture of the Tortonian suggest that part of this subsidence evolution was controlled by
350 E-W dextral strike-slip faults (Haughton, 2000; Baudouy et al., 2021) under transtensional strain.

Deleted: Romain

Deleted: Figs

Deleted: corridors

Deleted: Are

Deleted: The

Formatted: English (US)

Formatted: English (US)

Formatted: English (US)

Formatted: English (US)

Formatted: English (US)

Formatted: English (US)

Formatted: English (US)

Deleted: lower

Formatted: English (US)

Deleted: (~11-9 Ma)

Deleted: These continental deposits

Deleted: they

Deleted: directed

361 The transition from continental to deep marine sedimentary environments (water depth of 400-600 m according to
362 Poisson et al., 1999) witnesses the rapid rift-related tectonic subsidence achieved during the upper Tortonian times
363 (~9 Ma; **Figs. 6 and 7c**) (Augier et al., 2005b; Montenat and Ott d'Estevou, 1992; Wejermars et al., 1985). At around
364 8 Ma, accumulation rates drop by a factor of two to 200 m/Ma in HOB and 70 m/Ma in TB, revealing a marked
365 reduction in subsidence. Subsidence then became negative as basement uplifted from around 7 Ma (**Figs. 6b and 7d**)
366 in both TB and HOB.

367
368

Deleted: Romain

372 **Figure 6** : Stratigraphic evolution and lithologies of intramontane basins in the eastern Betics and offshore A1 well.
373 (a) Neogene stratigraphy and basin-fill correlation in the Almanzora and Huércal-Overa basins (Mora, 1993), Tabernas
374 basin (Hodgson and Haughton, 2004; Kleverlaan, 1989; Pickering et al., 2001) and Sorbas basin (Fortuin and
375 Krijgsman, 2003; Martin and Braga, 1994; Riding et al., 1998). Middle Miocene sedimentary environments in the
376 Alboran Sea are after (Comas et al., 1992). (b) Neogene tectonic subsidence evolution for Tabernas basin and Huércal-
377 Overa basin are from Augier (2004). The curves are obtained from backstripping techniques incorporating eustatic
378 and paleobathymetric corrections.

380 The geometry of the Almanzora (Pedrera et al., 2009), Sorbas (e.g. Do Couto et al., 2014) and Huércal-Overa basin
381 basins (Pedrera et al., 2010) inferred from gravity measurements indicate that these basins are asymmetrical and
382 deepening southwards. This sediment infill pattern recalls the formation of asymmetrical basins predicted by
383 numerical models of flexural strike-slip basins (Neuharth et al., 2021). According to this model, the asymmetry
384 observed should reflect the development of strike-slip basins loaded by sediments originated from the North. In
385 addition, a larger subsidence in HOB is an indication of abrupt crustal thinning to the south of Sierra de las Estancias
386 where the crustal thickness is the largest (Fig. 2). Therefore, at least the Serravallian-Tortonian infill patterns agree
387 with oblique extension.
388

Deleted: a

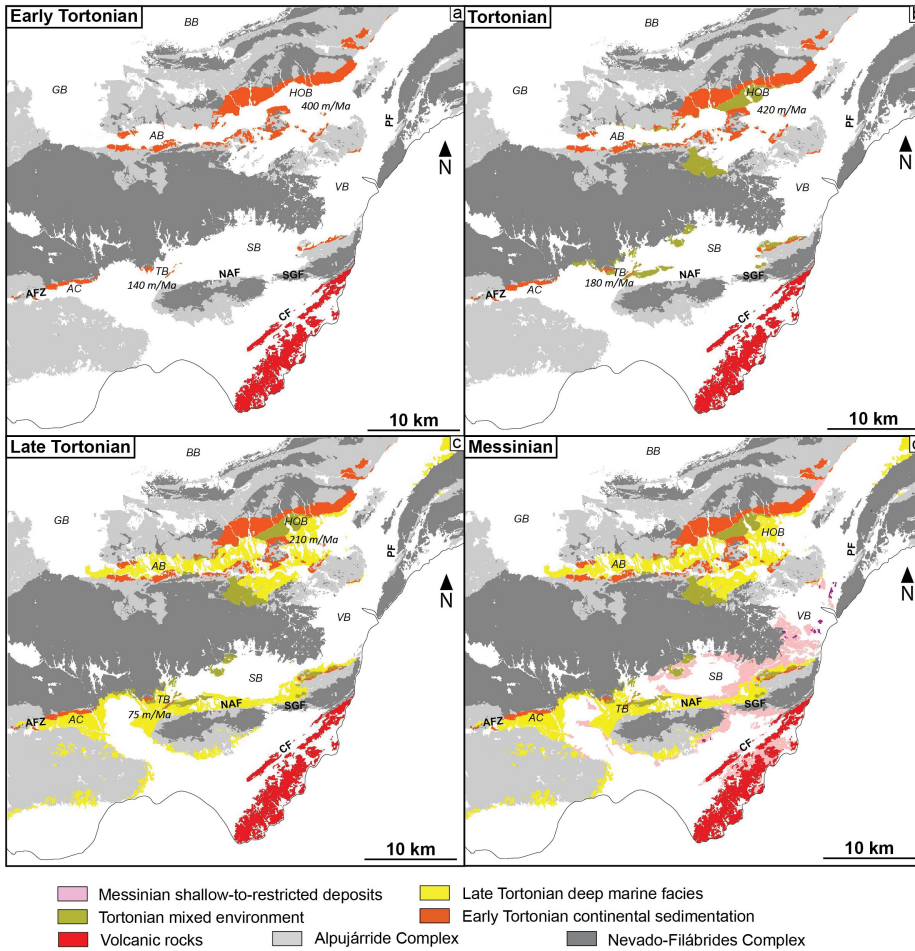
Deleted: (

Deleted: ,

Deleted: local

Deleted: (Fig. 5).

Deleted: of 35 km



395
396
397
398
399
400

Figure 7: Distribution of (a) lower Tortonian, (b) Tortonian, (c) upper Tortonian and (d) Messinian deposits based on geological mapping of the different basins. CF: Carboneras Fault; PF: P Fault; SGF: South Gafarillo fault; NAF: North Alhamilla fault; AFZ: Alpujarras fault zone; BB: Baza basin; GB: Guadix basin; AB: Almanzora basin; HOB: Huercal-Overa basin; VB: Vera basin; SB: Sorbas basin; TB: Tabernas basin; AC: Alpujarras Corridor.

Deleted: Palomeras

Deleted: corridor

401 4. Brittle faulting : pure extension versus transtensional deformation in Neogene basins

402 4.1. Tectonic regime in the eastern Betics

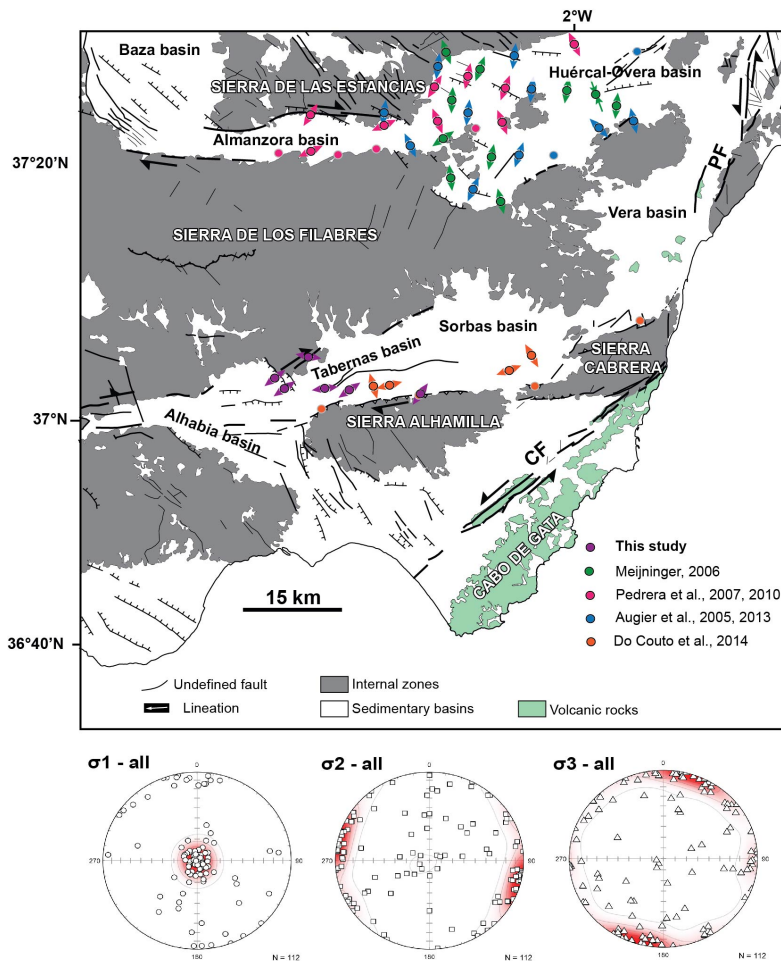
403 **Figure 8** presents a compilation of 112 fault slip data inversion previously analysed in the eastern Betics combined
404 with new measurements conducted in the Alpujarras Corridor and in the Tabernas basin (**Table S1**). Most faults are
405 syn-Tortonian or cut through the Tortonian. This compilation emphasizes a regional trend of σ_3 stress axes oriented

408 NNE-SSW (N20°E) with subordinate σ_3 oriented E-W. In details, this well-defined regional horizontal extension
409 reflects a combination of pure normal faulting regime (σ_2 horizontal and oriented NW-SE/WNW-ESE, 73% of stress
410 tensors) and strike-slip faulting regime (σ_2 vertical to steeply-dipping and σ_1 horizontal an striking NNW-SSE, 27%
411 of stress tensors). N-S to NW-SE compression is also reported in the HOB associated with incipient synform and
412 depocenter which is dated to the lower Tortonian coeval with the prominent EW/WSW-ENE extension (e.g. Pedrera
413 et al., 2010).

414 We describe below, based on a selection of outcrops in the vicinity of the contact between Tortonian basins and major
415 metamorphic domes, the expression of EW and NW-SE extensional faulting in the field. We then discuss how they
416 are linked to the regional stress regimes.

417

Deleted:).



419
420
421
422
423
424
425
426

Figure 8: Synthesis of stress regimes resolved from fault slip data inversion in Tortonian basins. Color-coded circles with arrows depict tectonic sites where extension (given as arrows) is horizontal (pure extensional or strike-slip stress regimes). Sites where reverse tectonic regimes prevail are shown as circles highlighted in grey. Below, stereoplots of paleostresses σ_1 , σ_2 and σ_3 show a compilation of all brittle tectonic regimes extracted from Table S1. Collectively they define a prominent extension oriented NNE-SSW with a subordinate E-W-striking extension. CF: Carboneras Fault; PF: Palomares Fault.

Deleted: Palomeras

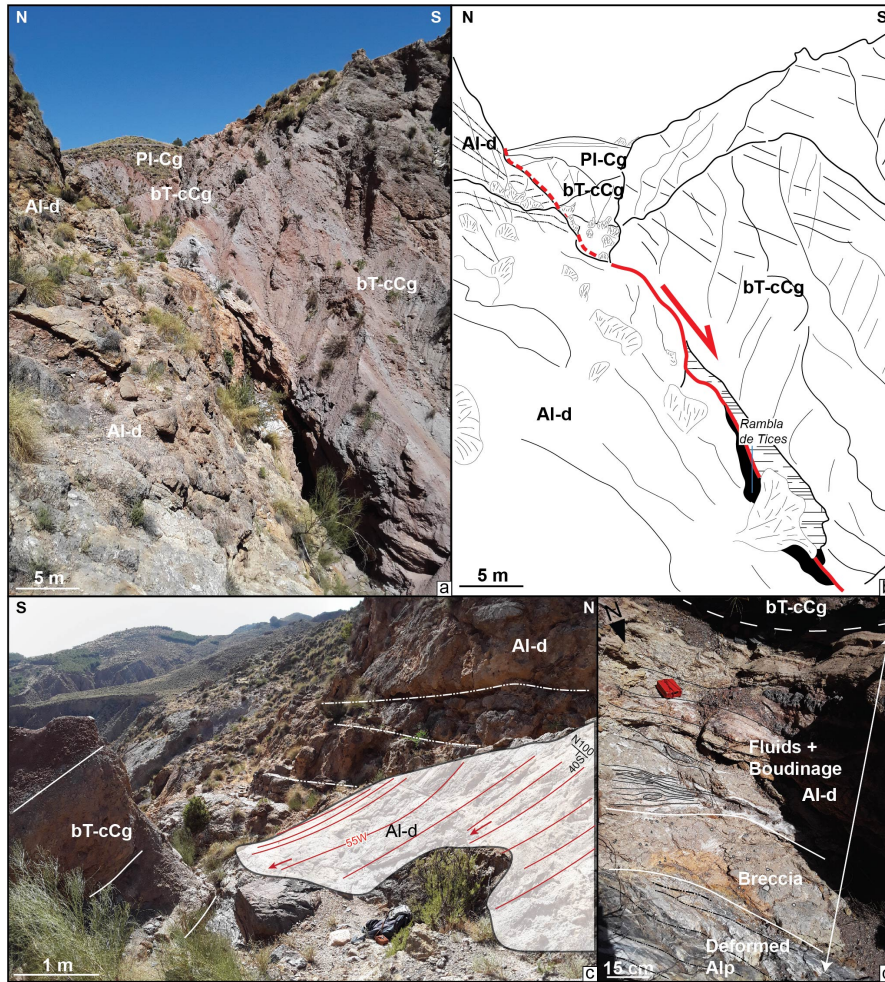
427
428
429
430

4.1 EW-directed faulting: evidence for pre-Tortonian oblique extension ?

In Tortonian intramontane basins, one of the main set of faults is represented by E-W-directed faults, including ENE-WSW to ESE-WNW sets. North of the Alpujarras Corridor (AC), 3 km to the NE of Canjáyar, the contact between the basal Tortonian conglomerates and the series of Alpujarride complex is exposed in the Rambla de Tices. It is

432 shaped by a 2-meter thick fault zone (**Figs. 9a,b**) striking N100°E, which has a normal sense of slip with a right-lateral
433 strike-slip component (**Fig. 9c**). It consists of cataclastic breccias and sheared blocks (boudins) of the host rocks (**Fig.**
434 **9d**). This major fault is found along the 65 km-long Alpujarras fault zone described by Martínez-Martínez (2006) as
435 a major strike-slip dextral transfer zone south of the Sierra Nevada that accommodates both WSW-extension and dextral
436 movement. It is mechanically consistent with NE-SW/ENE-WSW extension under a strike-slip regime as resolved
437 nearby along the same faults system (Martínez-Martínez, 2006). **Fig. 9** indicates the fault is parallel to the basal
438 Tortonian series but cuts across the Alpujarride complex. In the HOB, on the southern flank of the Sierra Limaria,
439 (**Fig. 8**), the unconformity between the lower Tortonian red conglomerates and the Alpujarride units (Rambla de
440 Cordoba, 2km NW Arboleas, **Figs. S1a, b**) is found reactivated as a normal fault with a dextral shear component.
441 To the North of TB, a large morphological surface presents a rare exposure of the micaschist basement of the Nevado-
442 Filabrides complex allowing the study of deformation on the southern flank of the Sierra de los Filabres (**Fig. 10**). The
443 deformed NF series shapes a kilometric-size antiform with axial planar surface dipping towards the North. The steeply-
444 dipping cleavages directed NE-SW on its southern flank are deformed by numerous dextral shear zones with lengths
445 ranging from 100 m to less than 5 m (**Fig. 10b, c**). In addition to isoclinal folds parallel to the main foliation that are
446 clearly associated to an early stage of ductile EW-stretching, we recognize close to the strike-slip shear zones, steeply-
447 dipping metric-size open to tight folds inclined to the NE (**Fig. 10d**). To the south, Tortonian conglomerates are
448 overlying unconformably the folded NF foliation. This stratigraphic relationships and the average low dip of Tortonian
449 strata (20°SE) indicate that strike-slip deformation occurred before the deposition of Tortonian conglomerates and
450 after the tilting of the NF foliation (see cross section in **Fig. 10a**). This argues that the transition from W-directed
451 ductile extension in the metamorphic domes known to have started in the Burdigalian and the right-lateral strike-slip
452 faulting occurred around the Langhian-Serravallian (13-14 Ma). This interval is often considered to mark the transition
453 from ductile to brittle extension (e.g. Augier et al., 2013). Because strike-slip faulting postdates folding of the NF
454 foliation, and are consistent with WSW-ENE oblique extension, we suggest that the Sierra de los Filabres metamorphic
455 dome formed in a transtensional strain regime. This hypothesis conforms with prediction of transtension at the tip of
456 the STEP fault (Le Pourhiet et al., 2012) and with model of oblique extension (see **Fig. 3**).
457

Deleted: ,



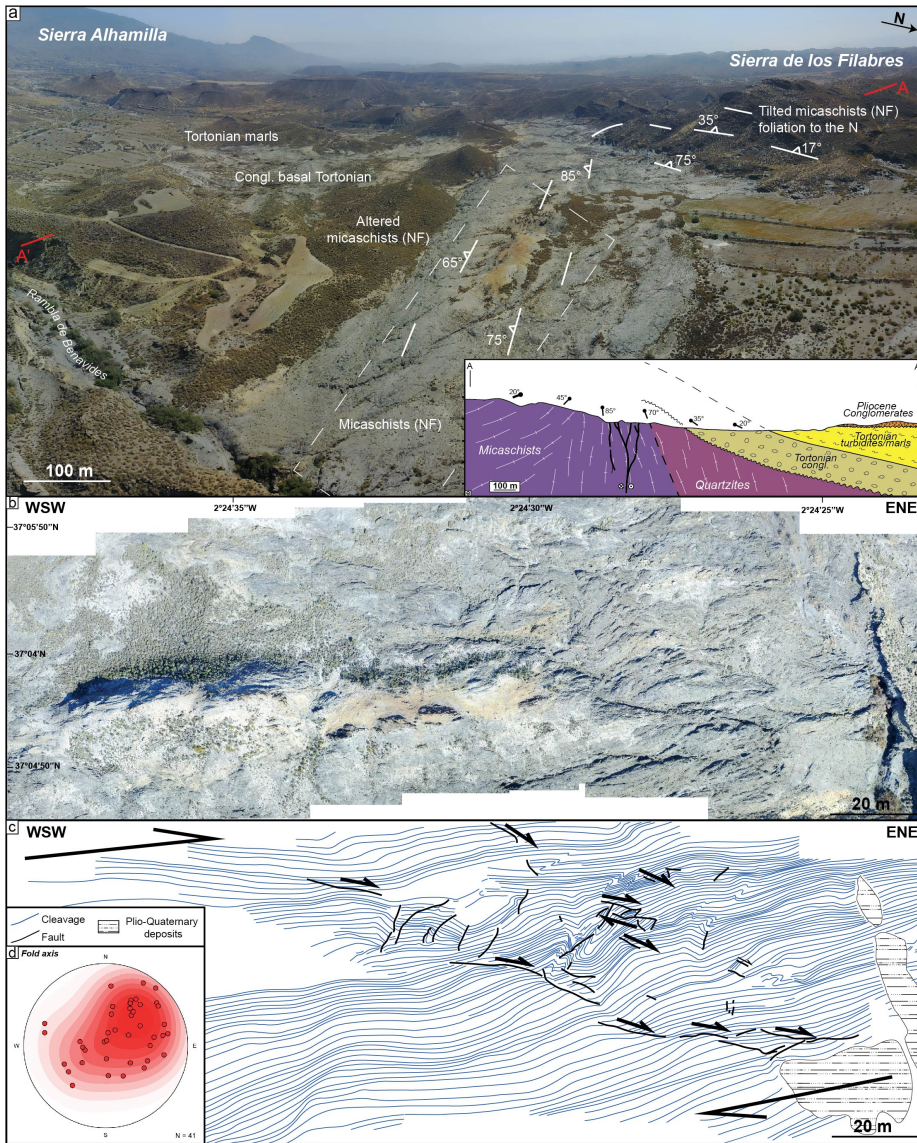
459
 460 **Figure 9.** (a) and (b) Fault zone at the contact between the Tortonian basal conglomerates and the series of the
 461 Alpujarride complex south of AC (Rambla de Tices, see Fig. 5 for location). (c) slickensides on the fault zone reveal
 462 a normal sense of slip with right-lateral strike-slip component found in association with (d) cataclastic breccias,
 463 sheared boudins of metamorphic and sedimentary rocks. Al-d: Alpujarride dolomites; bT-cCg: basal Tortonian
 464 continental Conglomerates; PI-Cg: Pliocene Conglomerates. Coordinates 37.031944°N/-2.716274°E.

466 **4.1.2. NW-SE-directed normal faulting**

467 A second set is represented by NW-SE directed normal faults (Fig. 8). They are found, for instance, bordering the the
 468 NE part of Alhabia basin, where they cut across the basement and interrupt the westward continuity of the southern

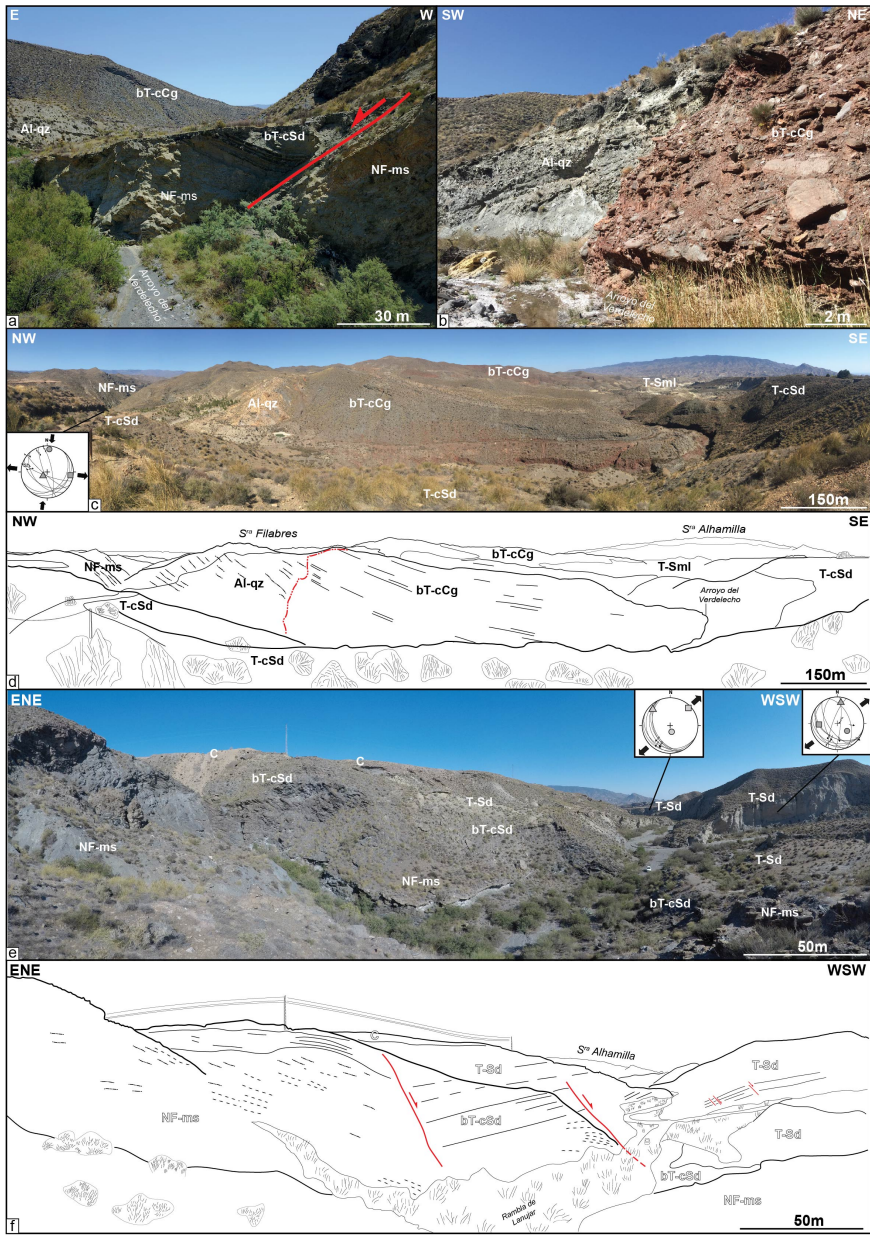
- Deleted: on
- Formatted
- Deleted: border of
- Formatted: English (US)
- Deleted: NW-SE
- Formatted: English (US)

472 [flank of the](#) Sierra de los Filabres. One major fault zone of this system is well exposed in the Arroyo del Verdelecho,
473 7 km to the west of Tabernas, on the eastern border of the Alhabia basin (**Figs. 11 and S2**). From a regional point of
474 view this large NW-SE fault zone controls the deepening of the Tortonian basin and the position of Pliocene
475 depocenter in its hangingwall, towards the West. NW-SE normal faults also cut across the lower Tortonian
476 conglomerates in the hangingwall but their throw diminishes upward in the upper Tortonian margin sediments,
477 suggesting fault activity during the late Tortonian (**Fig. 11**). One major fault zone is outlined by cataclastic breccias
478 made of marbles originated from the exhumed Alpujarride complex in the Sierra de los Filabres (**Fig. S2**).
479 South of HOB (south of Arboleas), NW-SE faults are seen cutting through the late Tortonian sands and marls series,
480 indicating that NE-SW extension is at least Tortonian (**Figs. S1c, d**).
481



482
 483 **Figure 10** : (a) Drone view taken in the SSW direction of the southern flank of the Sierra de los Filabres at the contact
 484 with the Tabernas basin (see Figure 5 for location). Local folding of the micaschist is apparent in the right where the
 485 foliation is striking NNE-SSW and is dipping ~25°E whereas it is vertical and striking SW-NE in the center of the
 486 studied area forming paleosurface. Local cross section highlights the unconformable contact between the Tortonian
 487 conglomerates and overlying on the basement. (b) High-resolution drone images of the paleosurface and (c) line-

488 drawing of the foliation revealing secondary folding (see **(d)** stereoplot of fold axes inclined to the NE) and dextral
489 shear zones. Coordinates 37.082777°N/-2.410544°E.
490
491
492



494 **Figure 11** : (a) Field photographs of a NW-SE normal fault at the contact between the Nevado-Filabride micaschists
495 (footwall) and Tortonian sediments (hanging wall). (b) Stratigraphic contact between grey and red basal Tortonian
496 continental conglomerates. These thick Tortonian series rest conformably on the Alpujarride complex (c, d).
497 Coordinates 37.059507°N/-2.478386°E. (e, f) NW-SE ~~normal~~ faults cutting across the NF micaschists basement.
498 These faults that also affect the early Tortonian deposits are sealed by late Tortonian deposits and are therefore syn-
499 depositional. See Figure 5 for location. Al-qz: Alpujarride quartzites; NF-ms: Nevado-Filabride micaschists; bT-cCg:
500 basal Tortonian continental Conglomerates; bT-cSd: basal Tortonian continental Sandstones; T-cSd: Tortonian coarse
501 Sandstones; T-Sd: Tortonian Sandstones; T-Sml: Tortonian Sandstones-marls; C: calcretes. Coordinates
502 37.061279°N/-2.490309°E. Paleostress orientations are in Table S1.
503

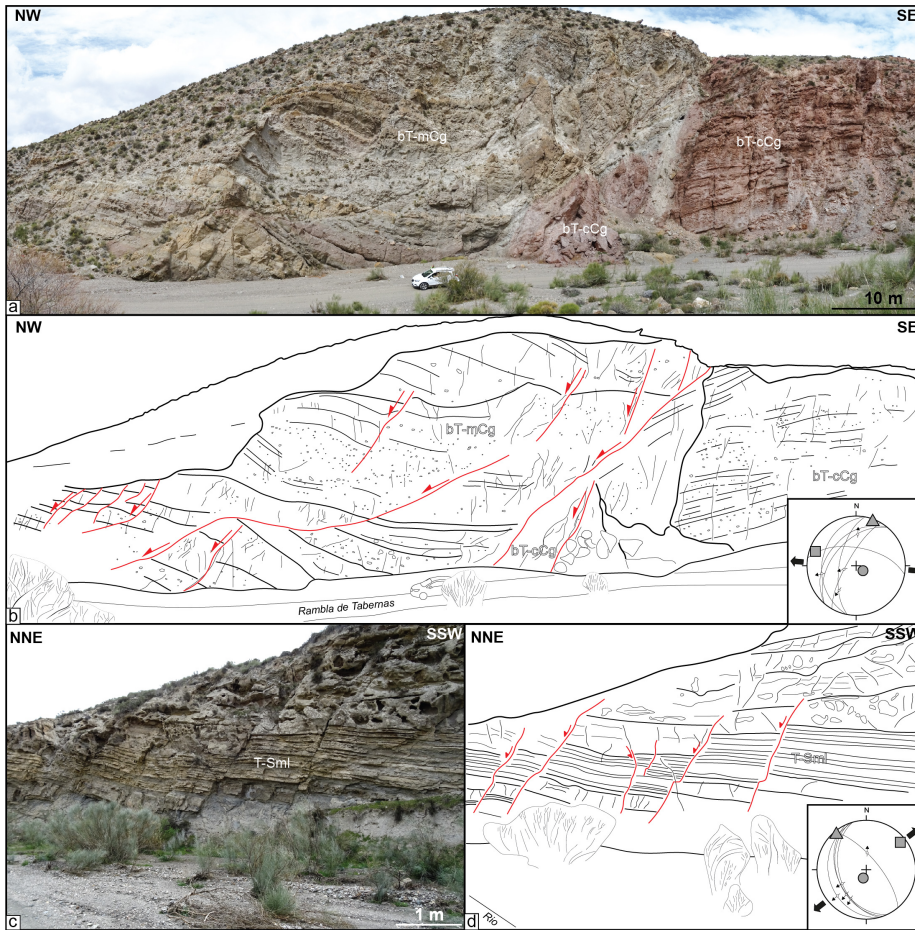
~~Deleted:~~ Normal

504 Both fault slip data and our own observations argue for a regional pre-Tortonian and syn-early Tortonian NNE-SSW
505 directed extension. This direction of extension is also found associated with less well-developed strike-slip regimes
506 (Fig. 8). It is consistent with the D1-D2 phase of brittle deformation found in HOB (Augier et al., 2013). The fact that
507 extension and strike-slip regimes occurred synchronously, or overlap rapidly in time, supports the view that they
508 reflect the same large-scale tectonic setting. The reason why strike-slip faulting is less apparent in the field than
509 expected in models in Fig. 3 is likely to reflect the fact that oblique extension is not fully partitioned between normal
510 and strike-slip components and is actually distributed along oblique structures. ~~Moreover~~, where strike-slip faults are
511 found they are associated with narrow basins or near the contact between the cover and basement but not in the center
512 of HOB or TB. The NNE-SSW to NW-SE faults appear to postdate the deposition of the early Tortonian red
513 conglomerates and is synchronous with the deposition of marine Tortonian series (Fig. 12). These normal faults
514 currently form half-graben filled with Plio-Quaternary deposits (Guadix, Baza, Alhabia) and are active today. But the
515 importance of extension-related brittle deformation over brittle compression decreases ~~eastwards~~. Indeed, a late brittle
516 compressional event oriented roughly N-S is described in the literature as a D3 brittle event (e.g. in HOB) associated
517 with reverse and strike-slip faults (Augier et al., 2013). The post-late Tortonian shortening is seen responsible for fold
518 amplification and reverse faulting on the northern limb of Sierra de Alhamilla and Sierra de los Filabres, and locally
519 in the eastern part of the HOB near the termination of left-lateral strike-slip faulting evolution of the Alhama de Murcia
520 fault (Fig. 8).

~~Deleted:~~ Moreover

~~Deleted:~~ corridor

~~Deleted:~~ eastwards



525
 526 **Figure 12:** (a, b) N-S to NNE-SSW-oriented normal to dextral faults affecting the basal Tortonian continental
 527 conglomerates (bT-cCg) and marine conglomerates (bT-mCg) (Rambla de Tabernas). They form a long and tight E-
 528 W anticlinal crosses the Tabernas basin (see Figure 5 for location). (c, d) Several normal faults observed in Tortonian
 529 sandstones and marls (T-Sml). They are mostly oriented NNW-SSE. Coordinates 37.041648°N/-2.399318°E.
 530 Paleostress orientations are in Table S1.

531 **5. N-S crustal-scale section across the oblique/transform margin of Alboran basin**

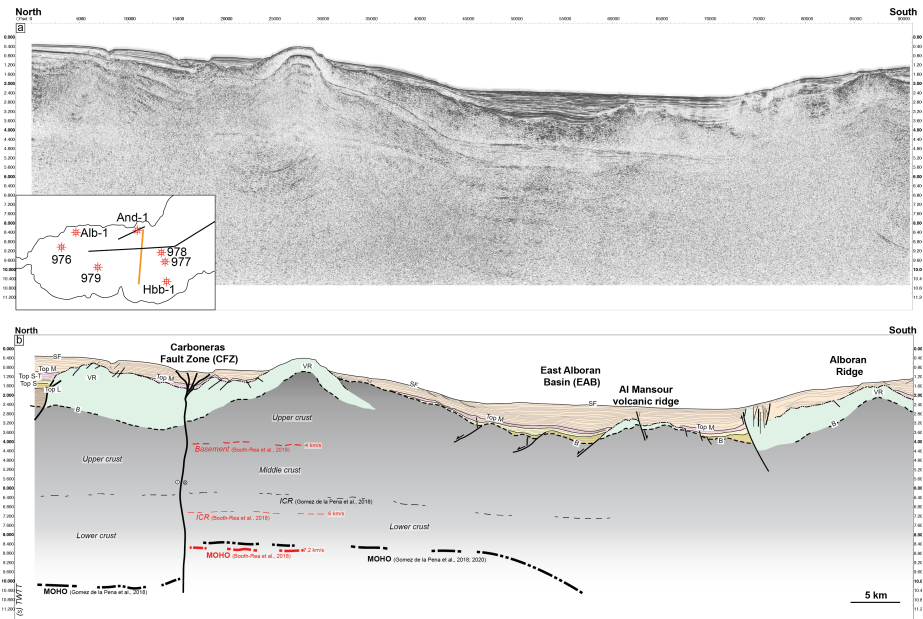
532 To examine further the structural relationships between extension and strike-slip faulting across the Alboran margin,
 533 we explore 2D multichannel seismic lines acquired during the MARSIBAL 1-06 cruise (Comas and MARSIBAL1-
 534 06 Scientific Party, 2007) and ESCI cruises (Comas et al., 1995) across the Eastern Alboran basin (EAB). The studied
 535 seismic dataset consists of ~300 km and are deep-penetration multichannel seismic reflection studies (12 s two-way
 536 travel time - TWTT). Here, we study two lines namely MSB08 and MSB07 (see location in Fig. 1). For stratigraphic

537 and structural correlations between the studied seismic lines, we used the Andaluca-A1 well (Fig. 6a) and results
 538 from ODP 977 and 978 legs (see location in Fig. 1). MSB08 is striking N70°E, slightly oblique to the shoreline. It is
 539 close, and runs parallel, to TM08 line of Gómez de la Peña et al. (2018). It is calibrated by Andaluca-A1 well and
 540 ESCI-Alb1 line (Comas et al., 1995). Line MSB07 stretches in the N-S direction between the EAB in Spain and SAB
 541 to the north of Morocco parallel to line TM09 (Gómez de la Peña et al., 2018) and crosscuts line ESCI Alb2b
 542 presented in Comas et al. (1995) and Booth-Rea et al. (2007) (Fig. 1).

544 **5.1 Offshore structures and stratigraphic architecture**

545 The Carboneras Fault is well imaged north of MSB07 (Fig. 13). It forms a positive crustal-scale antiformal flower
 546 structure related to left-lateral strike-slip faulting that involves a Moho depth variation between 12 s to 9-8 s TWT
 547 after Gómez de la Peña et al. (2018). It separates a thin continental crust to the North (25-20 km; Fig. 2), from the
 548 magmatic calc-alkaline arc crust of the EAB with a thickness of 18 km in the south (Booth-Rea et al., 2007, 2018;
 549 Gómez de la Peña et al., 2018, 2020a).

550



551
 552 **Figure 13** : Seismic reflection line MSB07 (location on Fig. 1). Discontinuous intracrustal reflectors (ICR) imaged
 553 between 3 and 6.5 s TWT, have been interpreted as mylonitic zones within the metamorphic basement (Carbonell et
 554 al., 1998; García-Dueñas et al., 1994; Gómez de la Peña et al., 2018). VR: Volcanic Ridge; B: Acoustic basement;
 555 Top L : Top Langian; Top S: Top Serravallian; Top S-T: top Serravallian-Tortonian; Top M: Top Messinian; SF:
 556 Seafloor.

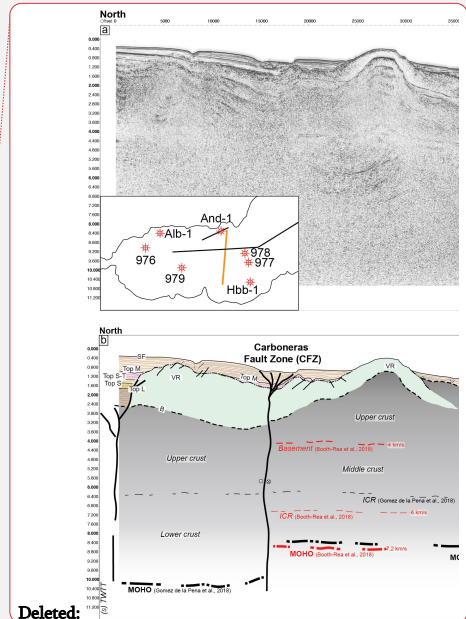
Deleted: (

Deleted: ..

Formatted: Font colour: Black, English (US)

Deleted: Gomez

Deleted: Gomez



Deleted:

Deleted: Gomez

563
564
565

566 Reflection seismic data (Figs. 13, 14, 15) collectively show a stratified crust, corresponding to the sediment cover,
567 down to 2.4-4 s TWT₁ which outlines the acoustic basement with high reflectivity (B). Locally, the top basement
568 reflector coincides with erosional palaeo-relief or high angle normal faults bounding basement highs. These faults are
569 oriented mostly NW-SE to NE-SW and cut across the basement. We recognized on seismic images magmatic additions
570 in the continental crust that are shaped by volcanic edifices exposed on the seafloor (e.g. Chella Bank) or slightly
571 buried (Alboran Ridge) outlined by symmetric downlaps and onlaps of sediments. These constructions form
572 topographic highs such as the Chella Bank on the MSB08 line (Fig. 14), the Alboran Ridge on the MSB07 line (Fig.
573 13) and the Maimonides Ridge on the ESCI-Alb2b line (Fig. 15). All the reflectors corresponding to layers as old as
574 Tortonian are onlapping against the volcanic ridges confirming that the volcanic activity occurred during the middle
575 to late Miocene times, which is shown by Duggen et al. (2008). Some reflectors up to the top Messinian (top M) onlap
576 onto the volcanic ridges probably as a result of Pliocene uplift.

Deleted: relatively well

577 The stratigraphy offshore, on the continental crustal domain, is defined by the recognition of five seismic stratigraphic
578 units in Andaluçia-A1 well (Jurado and Comas, 1992) labeled I-V from top to base (Figs 6 and 16) and separated by
579 unconformities. The seismostratigraphic units I to V vary in thickness (Fig. 16) and their architecture is conditioned
580 by the occurrence of basement highs and crustal-scale faults.

Deleted: otherwise

581 Below the Miocene sedimentary filling, Andaluçia-A1 well reveals ~190m of phyllitic and quartzitic meta-sediments
582 (2.4 to 4 s TWT below the Alboran basin, Figs. 13 and 14) topped by Langhian to Tortonian marls (top at ~1.6 to 3.4
583 s TWT below the Alboran basin) interbedded with Tortonian-Messinian tuffs and basaltic lavas. These units have
584 been correlated in the magmatic arc crust of EAB after Gómez de la Peña et al. (2020b). The older deposits (Unit V)
585 Langhian-Serravallian in age, consist of clays and marls with intercalated sands and volcano-clastic deposits. The
586 seismic facies of this Unit V is made of moderate amplitude and low frequency discontinuous reflections packages
587 (Figure 18), and is only present in the Northern Alboran Basin. They are correlated with volcanic series in the EAB
588 (vY3) (Gómez de la Peña et al., 2020b). They pass upward into Serravallian sand-silty clay turbidite (Unit IV) possibly
589 correlated with volcanic series in EAB (vY2 after Gómez de la Peña et al., 2020b). This unit exhibiting low to moderate
590 amplitude, moderate frequency drawing continuous sheeted to disrupted reflectors, is unconformably overlying Unit
591 V and locally onlaps onto the basement. Thickness of Unit IV remains rather thin in the North and East Alboran Basin.

Deleted: Gomez

592 It can't be properly identified in the South Balearic Basin, east of the Maimonides volcanic ridge (Fig. 15). The Unit
593 III dated from late Serravallian to late Tortonian is represented by sandstones interbedded with volcano-clastic levels
594 which correlates in EAB with volcanics vY1 unit. Unit III contains internal reflections characterized by low to moderate
595 amplitude, moderate frequency continuous sheeted reflectors. Its thickness remains relatively constant from the NAB
596 to the EAB, and is identified beneath the Messinian Unit II in the South Balearic Basin. Unit II corresponds to the
597 Messinian evaporite, carbonate, volcanic, and volcanoclastic deposits interbedded with fine-grained sediments and is
598 equivalent to unit III of Gómez de la Peña et al. (2020b) in EAB. Seismic facies of Unit II is marked in the Alboran
599 domain by lower amplitudes and lower frequency reflectors. In ESCI-Alb2b line, Unit II increases drastically east of
600 the Maimonides ridge, which delimits the western boundary of the salt deposits in the Western Mediterranean basin

Deleted: (Gomez

Deleted: Gomez

Deleted: (

Deleted: ..

611 during the Messinian Salinity Crisis (Haq et al., 2020). Unit II is topped by Unit I made of Pliocene to Quaternary
 612 clays and sanstones, which are correlated with units II and I in EAB (Gómez de la Peña et al., 2020b). Unit I is marked
 613 by thinly bedded, mostly parallel, high-frequency and low amplitudes reflectors (Fig. 15). Its thickness fluctuates in
 614 response to sedimentary processes (Juan et al., 2016).

615 Along line MSB08 (Fig. 14) the Langhian-Serravallian (Unit V) is maximum 1600 m-thick (using a P-wave velocity
 616 of 3.2 km/s calculated within Andalusia-A1 well). In EAB, south of Carboneras Fault Zone, the total thickness of Unit
 617 V is only ~300 m on MSB07 (Fig. 13) and is absent in ESCI-Alb2b (Fig. 15). The Serravallian-Tortonian (Unit IV-
 618 III) interval shows only very limited sediment accumulation (~300 m) except near the NW-SE oriented normal faults
 619 where growth geometries are visible. These normal faults are sealed by the Tortonian-Messinian deposits, indicating
 620 a syn-sedimentary faulting during the middle Miocene (Fig. 13). With respect to onshore observations this
 621 sedimentary infill is more continuous and is also much thinner compared to TB and HOB where they are represented
 622 by thick conglomerates and marls/turbidites (> 1km) (Fig. 7), and they are eroded or not deposited along the axes of
 623 the metamorphic domes. The Messinian deposits (Unit II) are ~150-350 m-thick north of CF (MSB07-08 ; Figs. 13,
 624 14) and increase to about 1200 m eastward in the eastern EAB (ESCI-Alb2b ; Fig. 15), and in Algero-Balearic basin
 625 (Gómez de la Peña et al., 2020b). The top Messinian reflector is topped by thick horizontal sedimentary strata, with a
 626 maximum thickness of 1.2 s TWT (~2.4 km assuming a velocity of 2 km/s) on line MSB07, suggesting an important
 627 channel system during the Pliocene.

628 The Pliocene-to-Quaternary series are poorly deformed except in the vicinity of CF and near the Alboran Ridge where
 629 this is associated with south-dipping reverse fault (Fig. 13). This late and still active compressional tectonics is
 630 revealed by the overthrusting of the SAB over the south margin of the EAB (e.g. Martínez-García et al., 2011).
 631

Deleted: Gomez

Deleted: 18

Deleted: .

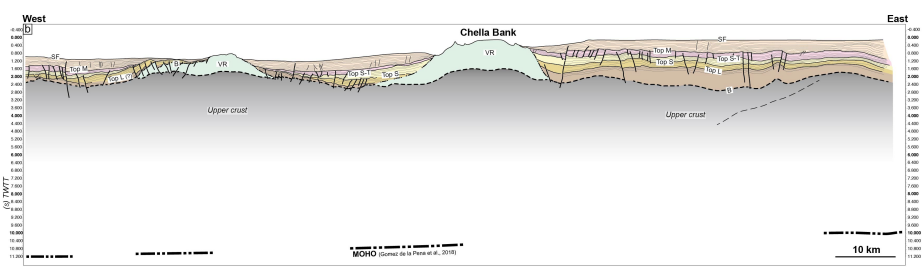
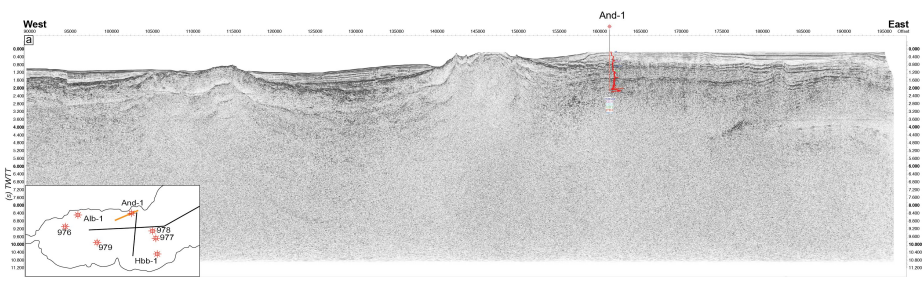
Deleted: offshore

Deleted: compared

Deleted: Gomez

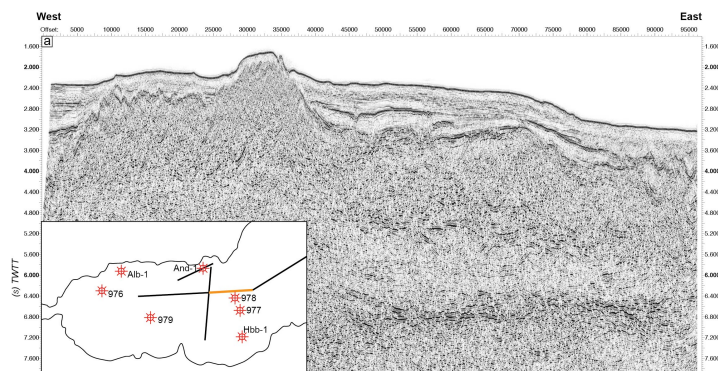
Deleted: (

Formatted: English (US)

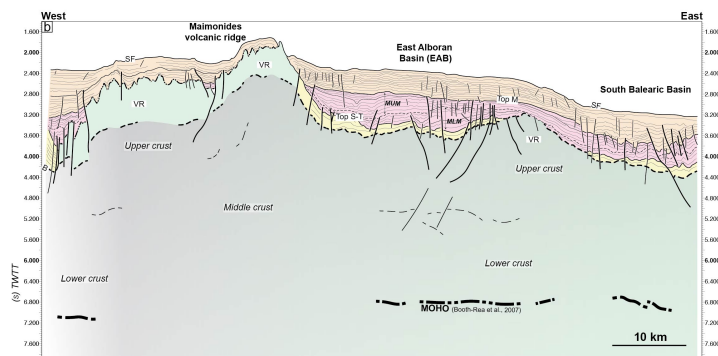


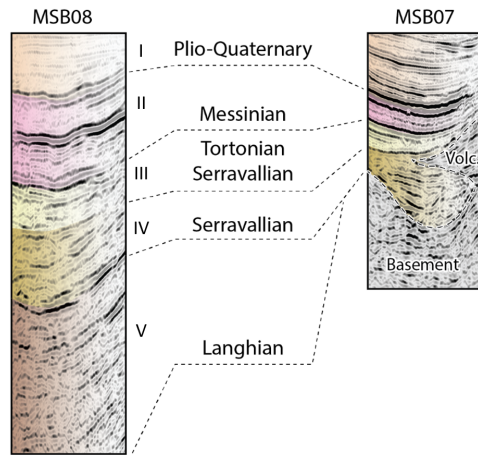
632

640 **Figure 14** : Seismic reflection line MSB08 (see location on **Fig. 1**). See Figure 13 for abbreviations. See also Figure
 641 S3 showing a zoom on the main seismic facies recognized in Andalucia-A1 well.
 642



643 **Figure 15. (a, b)** Seismic reflection line ESCI-Alb2b and interpretation (see Figure 1 for location). Seismic units are
 644 correlated with those defined by Booth-Rea et al. (2007). See Figure 13 for abbreviations.
 645
 646
 647





648
649 **Figure 16** : Seismic facies of units I to V seen through seismic lines MSB08 close to the shoreline and the line
650 MSB07, located deeper in the East Alboran Basin.

651 **5.2 N-S crustal cross-section of the Alboran margin accounting for strike-slip faulting**

652 Based on subsurface constraints and field data, we present in Figure 17 a crustal-scale section across the rifted margin
653 from the Sierra de las Estancias and Huercal-Overa basin (HOB) to the Alboran ridge that represents the inverted
654 southern margin of the EAB (Fig. 17). The proximal margin, where the crust is 30-35 km-thick, is defined to the North
655 by the transition between the south Iberia margin, and the metamorphic domain of the Alboran basement exposed in
656 the Sierra de las Estancias. This continental domain preserves part of the crustal thickness acquired during former
657 Betic orogenic phase that has been little involved in crustal thinning. The onset of crustal thinning to the south
658 coincides with the position of the lithospheric tear fault documented by seismology (Fig. 4; Mancilla et al., 2015a)
659 and is recorded by the formation of asymmetric basins of the HOB and TB, shaping the upper neck domain. Orthogonal
660 and oblique extension in this domain is accommodated by normal and strike-slip faulting during the Tortonian. From
661 the Sierra de los Filabres to the south, the thickness of the continental crust reduces to 25 km in the Tabernas basin
662 along the Alpujarras strike-slip fault zone and below the Sierra Alhamilla (Fig. 17). The Nijar basin depicts the
663 transition towards offshore distal domains where the continental crust reaches a thickness of 20 km. The Tortonian
664 and Messinian marine sediments are also thicker. It is worth noting that a number of volcanic bodies offshore (e.g.
665 Chella Bank on MSB08) accompany crustal thinning of the continental crust. The Carboneras Fault (CF) brings crusts
666 with different thicknesses and composition into contact. South of CF, the crustal thickness of the EAB is 18 km and
667 seismic velocities, especially the occurrence of a high-Vp lower crust, has been considered to indicate the EAB is
668 floored by a magmatic arc crust (Gómez de la Peña et al., 2018; 2020), formed in a supra-subduction context above
669 the subducting Alboran slab (Booth-Rea et al., 2018). The crustal thickness of the EAB is compatible with crustal
670 thinning of the continental margin, and the occurrence of NW-SE-trending faults also recognized onshore despite
671 being slightly older (Serravalian-Tortonian) suggest that the EAB formed under the same back-arc extension setting.

- ~~Deleted:~~ have built
- ~~Deleted:~~ cross-
- ~~Deleted:~~), which
- ~~Formatted:~~
- ~~Deleted:~~ proximal
- ~~Deleted:~~ , to the center
- ~~Deleted:~~ Alboran margin
- ~~Formatted:~~
- ~~Formatted:~~ English (US)
- ~~Formatted:~~ English (US)
- ~~Formatted:~~ English (US)
- ~~Deleted:~~ a 30-35 km-thick crust. It
- ~~Deleted:~~ strongly subsident and
- ~~Deleted:~~ This domain is characterized by orthogonal
- ~~Deleted:~~ during the Tortonian
- ~~Deleted:~~ . This boundary also corresponds to the position of the major STEP fault documented by seismology.
- ~~Deleted:~~ crustal
- ~~Formatted:~~ English (US)
- ~~Deleted:~~ corridor
- ~~Deleted:~~ .
- ~~Formatted:~~ English (US)
- ~~Deleted:~~ with
- ~~Formatted:~~ English (US)
- ~~Deleted:~~ crustal
- ~~Formatted:~~ English (US)
- ~~Deleted:~~ and
- ~~Formatted:~~ English (US)
- ~~Deleted:~~ . Crustal thinning appears localized along the
- ~~Deleted:~~), which juxtaposed crust
- ~~Deleted:~~ crustal thickness (Fig. 19).
- ~~Deleted:~~ crust
- ~~Deleted:~~ reduces below 20
- ~~Formatted:~~ English (US)
- ~~Formatted:~~ English (US)
- ~~Deleted:~~ shows increasing magmatic additions making
- ~~Deleted:~~ of the EAB (Gomez
- ~~Deleted:~~
- ~~Deleted:~~ . Interestingly, normal faulting in the EAB is sealed
- ~~Formatted:~~ ... [2]
- ~~Deleted:~~ deposits. Crustal deformation then shifted

702
703
704
705
706
707
708
709

710
711
712
713
714
715
716

relative to westward slab retreat as the whole Alboran margin did. Thus, the magmatic arc crust of the EAB could represent voluminous magmatic intrusions (e.g. Al Mansour dacite, Alboran Ridge rhyolite dated to ca. 9 Ma; Duggen et al., 2004; Fig 17) formed on the distal rifted margin of Alboran. The investigation of the causes of calc-alkaline magmatism is beyond the scope of this study, but we suspect it reflects post-subduction arc magmatism induced by remelting, during extension or delamination, of a metasomatized wedge of mantle lithosphere formed during a previous subduction event (e.g. Richards, 2009). Crustal shortening in Figure 17 is distributed across the CF and EBSZ strike-slip fault zones, north-vergent reverse faults below the Alboran Ridge and on the northern limb of Sierra de Alhamilla.

Formatted: English (US)
Deleted: the north in

Deleted: and to the south along the Alboran Ridge where
Deleted: faulting occurred

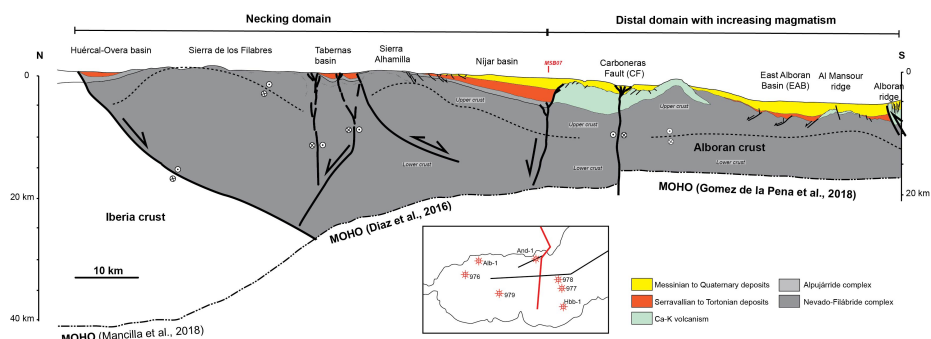


Figure 17. Crustal-scale cross section of the Alboran margin in the eastern Betics interpreted based on onshore and offshore constraints presented in the text. Note that in the necking domain the extension of faults downwards to Moho depths is not imaged on the seismics and therefore largely inspired by inferences from 3D numerical models (see Fig. 3).

720 **6. Implications**

721 The question of whether the Miocene tectonic evolution of the Betics reflects crustal thinning associated with oblique
722 back-arc rifting as suggested from present-day strain patterns is unclear in the literature. We found based on a
723 comparison between numerical models and basin analyses, fault kinematics and structure of the margin in the eastern
724 Betics compelling evidences that crustal thinning was controlled by oblique extension. Oblique rifting operated since
725 at least the middle Miocene, in relation with Alboran slab retreat below the Alboran basin and is kinematically
726 associated with slab tearing and delamination below the central and eastern Betics.
727 One of the most striking tectonic feature of the Alboran margin (Fig. 17) is the abrupt N-S crustal thinning oblique to
728 the direction of slab rollback. The history of sediment infill and rates of subsidence in intramontane basins (Figs. 6
729 and 7) combined with the analyses of fault slip data, and structural data offshore, confirm that brittle extension
730 oriented from N20°E to EW occurred during an interval spanning from the Serravallian-early Tortonian to the late
731 Tortonian (14-8 Ma) (Fig. 18). This extension is found associated with both normal and strike-slip regimes. Field
732 tectonic data reveal that N20°E extension is more represented in HOB, while the ENE-WSW to EW extension is found
733 related with the evolution of the Almanzora fault zone, Alpujarras fault zone and Tabernas basin flanking the
734 metamorphic domes (Table S1). There are additional evidence that EW-directed dextral strike-slip faulting occurred
735 during the Tortonian to the South and West of the HOB. These large-scale transfer fault zones positioned on the slab
736 edge accommodate the differential westward extension that are later cut by Tortonian NW-SE faults. These second
737 set of faults is also observed in the magmatic crust of the EAB offshore but seismic data indicate they are Serravallian-
738 Tortonian in age and therefore older than those identified onshore. We suggest that NW-SE normal faulting could
739 have initiated in the EAB then migrated towards the necking domain, which was dominated by transfer faulting, as
740 slab retreat progressed and the region affected crustal thinning widened (Fig. 18). Subsidence during the Serravallian-
741 Tortonian was also lower in the magmatic crust of the EAB compared to intramontane basins onshore. This suggest
742 that the isostatic effect of crustal thinning was compensated by a thermal anomaly in the mantle, heralding the Ca-K
743 magmatism at 11-7 Ma (Duggen et al., 2004, 2008).

Deleted: 7

Deleted: Back-arc extension, recent tectonic inversion and STEP faulting are generally considered to result from separated processes.

Deleted: of basin evolution

Deleted: occurred under

Deleted: and was not restricted to the post-Tortonian evolution. Rather, oblique

Deleted: possibly

Deleted: , as the

Deleted: started in

Deleted: therefore

Deleted: STEP faulting.

Deleted: , from 35-30 km to 25-20 km,

Deleted: retreat

Deleted: In more details, these

Deleted: suggest

Deleted: ,

Deleted: corridor

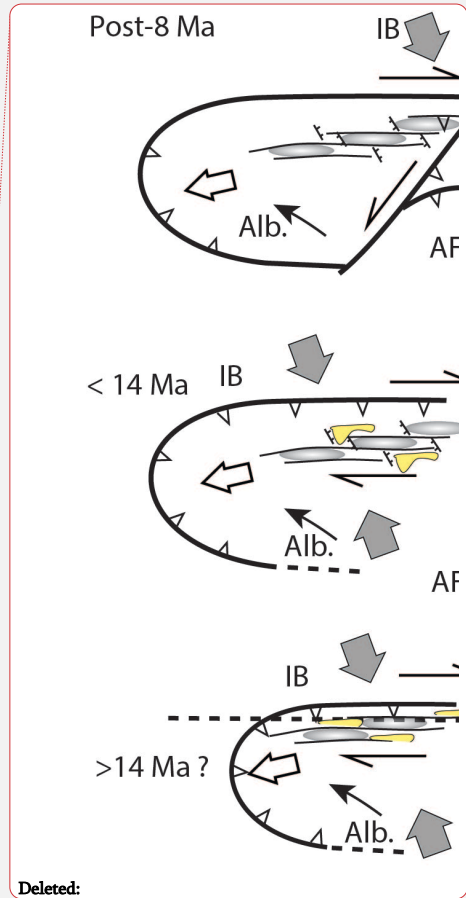
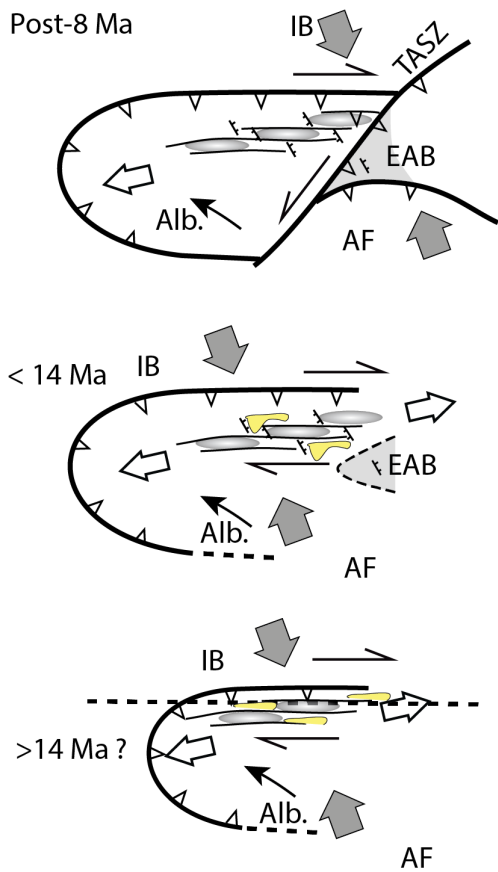
Deleted: corridor

Deleted: Tarbenas

Moved (insertion) [1]

Deleted: did occur during the Tortonian to the South and West of the HOB and represents this main phase of basin subsidence. These large-scale faults are later cut by Tortonian NW-SE faults that argue for more recent EW extension. Therefore, we infer that the domain south of the HOB, which also corresponds to a thinnest crust, has experienced transensional deformation and EW extension.

Formatted: Font colour: Black



773

774 **Figure 18:** Tectonic model of the evolution of the northern margin of the Alboran Rift. Large grey and white double
 775 arrows depict shortening, which is parallel to the AF/IB convergence, and the highly oblique extension, respectively.
 776 The thin black arrows show the motion of Alboran relative to Iberia (IB) taken from Figure 4. Half arrows depict
 777 distributed strike-slip faulting in the Betics. NW-SE directed normal fault and strike-slip basins (yellow) are
 778 consistent with the oblique extension. Grey-shaded ellipses represent the metamorphic domes. TASZ : simplified
 779 representation of the Trans-Alboran Shear Zone. We also indicated EAB which mostly formed ca. 9 Ma (Duggen et
 780 al., 2004; Booth-Rea et al., 2018).
 781

782 Several key tectonic features found in the eastern Betics are predicted by 3D models of oblique extension (Figure 3).
 783 They include E-W trending normal faults that are prevalent on the upper neck domain (i.e. Sierra de las Estancias and
 784 HOB), and E-W strike-slip faults (Almanzora and Alpujarras fault zones). NW-SE normal faults are associated with

- Deleted: is showing
- Deleted: depicts the
- Deleted:
- Deleted: specific
- Deleted: Those
- Deleted: the
- Deleted: corridor) and
- Deleted: that
- Deleted: found

795 more distal domains on the continental margin where crustal thinning is the highest offshore, south of Nijar basin, and
796 in the EAB.
797 Tectonic inversion seems, in contrast, to have been increasingly more important when approaching the Carboneras
798 and Palomares strike-slip faults in the East since the late Tortonian.
799 Ductile thinning associated with the formation of metamorphic domes and exhumation of HP rocks is dated to 23 to
800 16 Ma (Platt et al., 2006; Booth-Rea et al., 2015). This provides time constraint for the beginning of oblique extension
801 and westward slab rollback. Deformation at the future location of the tear fault was probably initially diffuse and
802 resulted in an immature oblique rift system in the South, combined with thrusting in the external zones to the North
803 (Figure 18). In the Langhian-Serravallian (14-13 Ma), accompanying slab steepening, localization of slab tearing, and
804 propagation of thrusting in external zones, oblique extension spread over the whole central Betics. At this time,
805 metamorphic domes exhumed to upper crustal levels and recorded the transition from ductile shearing to brittle
806 faulting (Figure 18). Brittle E-W-directed stretching and dextral transcurrent deformation formed at this time. The
807 late/post-Tortonian times (~8 Ma) marks a change in the tectonic evolution of the Betics and Alboran domain as the
808 mantle slab detached with no further westward slab retreat (van Hinsbergen et al., 2014; Do Couto et al., 2014;
809 Martínez-García et al., 2017; d’Acremont et al., 2020; García-Castellanos and Villaseñor, 2011; Spakman et al., 2018).
810 This regional event is synchronous with the cessation of extension and onset of uplift in the western Mediterranean
811 region and Iberia (Jolivet et al., 2021a; Mouthereau et al., 2021; Rat et al., 2022). Ca-K magmatism occurred between
812 11 and 7 Ma and was followed, east of EBSZ, by the indentation by the magmatic crust of the EAB in the Águilas
813 Arc (Ercilla et al., 2022), and amplification of the metamorphic domes in the vicinity of the EBSZ (e.g. Alhamilla)
814 (Figure 18).
815 In this model, ductile stretching and ductile detachment associated with the development of the domes are the
816 expression of oblique E-W extension. It provides a coherent scheme linking the formation of EW-directed basins in
817 the brittle field associated with strike-slip faulting, and NW-SE/NNW-SSE sedimentary basins (Guadix, Baza,
818 Alhabia) formed in transtension during the Tortonian. As such, the oblique extension is closely associated with STEP
819 faulting required by westward slab rollback. The oblique rifting model we propose explain the formation of the
820 metamorphic domes and intermontane basins and provides insight into crustal deformation, which is broadly
821 consistent with the geodynamic models of slab rollback and tearing since 20 Ma that have been previously proposed
822 for Alboran (Chertova et al., 2014; Spakman et al., 2018). In the latter models, however, the ENE-WSW extension in
823 the central-eastern Betics is related to differential absolute motions between Iberia and the slab decoupled from Iberia
824 by slab tearing. In our scenario, oblique extension is entirely related to westward lateral rollback. It can not be
825 excluded, however, that the effect of mantle-derived slab dragging increased during the late extensional stage, from
826 14-13 Ma, when slab tearing localized.
827 Mid-Miocene high-pressure metamorphism, documented in the central Betics (Platt et al., 2013) was synchronous with
828 slab steepening and subduction that was under way during oblique back-arc extension (Figure 18). The case of
829 exhumation of high-pressure rocks in oblique convergence setting associated with near-parallel orogen extension is
830 also documented in other active orogen like Taiwan (Conand et al., 2020).

Deleted: Brittle E-W-directed stretching and dextral transcurrent deformation started

Deleted: Langhian-Serravallian (14-13 Ma).

Deleted: Palomeras

Deleted: According to temporal constraints, ductile thinning may have occurred between 23 to 16 Ma prior to brittle faulting at 14-13 Ma (Figure 18). The late/post-Tortonian times marks a change in the tectonic evolution of the region (Jolivet et al., 2021a; Mouthereau et al., 2021; Rat et al., 2022) as the mantle slab eventually detached and is responsible for Ca-K magmatism at 11-7 Ma (Duggen et al., 2008, 2004), compression and tightening of the metamorphic domes associated with the formation of the the EBSZ. The strike-slip deformation model has the advantage to explain N-S crustal thinning in the Betics while back-arc extension is oriented E-W, in a continuum of deformation from the Miocene to the present.

Deleted: This

Deleted: , which

Deleted: retreat, is overall a characteristic feature

Deleted: regional NW-SE/NNW-SSE convergence since at least the Miocene. Only recently, around 8 Ma, as

Deleted: detached, shortening started to prevail

Deleted: vicinity of the EBSZ (Figure

Moved up [1]: 18).

Deleted: As convergence was under way during oblique back-arc extension,

Deleted: and subduction possibly occurred during the mid-Miocene as argued

Deleted: eastern

Deleted:). Moreover, the

Deleted: orogeni

863 This highly oblique northern Alboran margin differs from typical transform fault margin such as those associated with
864 the Atlantic ocean because it accommodates variations in intra-plate extensional movements, triggered by slab roll-
865 back, not variations in spreading rates. Strike-slip faults may have originated as low-angle normal faults which were
866 later reactivated as thrusts during margin inversion. Similar observations, including metamorphism, strike-slip
867 faulting, high geothermal gradients and volcanism has been made in Seram, north of the Banda Arc, which represents
868 another example of extremely thinned crust formed perpendicular to the direction of the slab rollback (Pownall et al.,
869 2013). Such a narrow rifted margin associated with lithospheric STEP fault defines a class of oblique margin that is
870 expected to be hardly preserved in the geological record due the transient nature of retreating subduction systems.

Deleted: an other

Deleted: retreat

Deleted: (and transform)

871
872

873 **Data availability.** This study is based on data compilation. Data used in this study can be found in the appropriate
874 references. Paleostress tensors obtained by the inversion of fault slip data are available online in the Supplement.

875

876 **Supplement.** The supplement related to this article is available on-line at:

877

878 **Competing interests.** The authors declare that they have no conflict of interest.

879 Authors contribution

880 ML and FM, conceptualize, prepared figures and tables, compiled and interpreted field structural data and wrote the
881 paper. DC provided and interpreted the seismic lines, reviewed the text and contributed to the writing. AJ carefully
882 examined the implementation of his numerical results and reviewed the text. EM, SC and VM, supervised and
883 coordinate the different project tasks and reviewed the text.

884 Acknowledgments

885 Victor Tendero Salmerón, Guillermo Booth-Rea, and an anonymous reviewers are warmly thanked for their comments
886 that greatly improved the manuscript. The stereogram results were obtained using Win-Tensor, a software developed
887 by Dr. Damien Delvaux, Royal Museum for Central Africa, Tervuren, Belgium (Delvaux and Sperner, 2003). The
888 processed seismic data were interpreted using Kingdom IHS Suite© software. This research benefited from
889 discussions and support of OROGEN project, an academic-industry research consortium between TOTAL, CNRS and
890 BRGM.

891

892

896 **References**

- 897 Angrand, P., Mouthereau, F., 2021. Evolution of the Alpine orogenic belts in the Western Mediterranean region as
 898 resolved by the kinematics of the Europe-Africa diffuse plate boundary. *Bsgf - Earth Sci Bulletin*.
 899 <https://doi.org/10.1051/bsgf/2021031>
- 900 Argus, D.F., Gordon, R.G., DeMets, C., 2011. Geologically current motion of 56 plates relative to the no-net-
 901 rotation reference frame. *Geochemistry, Geophysics, Geosystems* 12. <https://doi.org/10.1029/2011gc003751>
- 902 Augier, R., 2004. Evolution tardi-orogénique des Cordillères Betiques (Espagne) : apports d'une étude intégrée 1
 903 vol., [II]-400 p.
- 904 Augier, R., Agard, P., Monié, P., Jolivet, L., Robin, C., Booth-Rea, G., 2005. Exhumation, doming and slab retreat in
 905 the Betic Cordillera (SE Spain): in situ ⁴⁰Ar/³⁹Ar ages and P–T–t paths for the Nevado-Filabride complex.
 906 *Journal of Metamorphic Geology* 23, 357–381. <https://doi.org/10.1111/j.1525-1314.2005.00581.x>
- 907 Augier, R., Booth-Rea, G., Agard, P., Martínez-Martínez, J.M., Jolivet, L., Azañón, J.M., 2005a. Exhumation
 908 constraints for the lower Nevado-Filabride Complex (Betic Cordillera, SE Spain): a Raman thermometry and
 909 Tweek multiequilibrium thermobarometry approach. *Bulletin de la Societe Geologique de France* 176, 403–
 910 416. <https://doi.org/10.2113/176.5.403>
- 911 Augier, R., Jolivet, L., Couto, D.D., Negro, F., 2013. From ductile to brittle, late- to post-orogenic evolution of the
 912 Betic Cordillera: Structural insights from the northeastern Internal zones. *Bulletin De La Société Géologique De*
 913 *France* 184, 405–425. <https://doi.org/10.2113/gssgfbull.184.4-5.405>
- 914 Augier, R., Jolivet, L., Robin, C., 2005b. Late Orogenic doming in the eastern Betic Cordilleras: Final exhumation
 915 of the Nevado-Filabride complex and its relation to basin genesis. *Tectonics* 24, n/a-n/a.
 916 <https://doi.org/10.1029/2004tc001687>
- 917 Badji, R., Charvis, P., Bracene, R., Galve, A., Badsí, M., Ribodetti, A., Benaissa, Z., Klingelhofer, F., Medaouri,
 918 M., Beslier, M.-O., 2014. Geophysical evidence for a transform margin offshore Western Algeria: a witness of a
 919 subduction-transform edge propagator? *Geophys J Int* 200, 1029–1045. <https://doi.org/10.1093/gji/ggu454>
- 920 Baudouy, L., Houghton, P.D.W., Walsh, J.J., 2021. Evolution of a Fault-Controlled, Deep-Water Sub-Basin,
 921 Tabernas, SE Spain. *Frontiers Earth Sci* 9, 767286. <https://doi.org/10.3389/feart.2021.767286>.
- 922 Bessière, E., Jolivet, L., Augier, R., Scaillet, S., Précigout, J., Azañón, J.-M., Crespo-Blanc, A., Masini, E., Couto,
 923 D.D., 2021. Lateral variations of pressure-temperature evolution in non-cylindrical orogens and 3-D subduction
 924 dynamics: the Betic-Rif Cordillera example. *Bsgf - Earth Sci Bulletin*. <https://doi.org/10.1051/bsgf/2021007>
- 925 Bezada, M.J., Humphreys, E.D., Toomey, D.R., Harnafi, M., Dávila, J.M., Gallart, J., 2013. Evidence for slab
 926 rollback in westernmost Mediterranean from improved upper mantle imaging. *Earth and Planetary Science*
 927 *Letters* 368, 51–60. <https://doi.org/10.1016/j.epsl.2013.02.024>
- 928 Booth-Rea, G., Martínez-Martínez, J.M., Giaconia, F., 2015. Continental subduction, intracrustal shortening, and
 929 coeval upper-crustal extension: P-T evolution of subducted south Iberian paleomargin metapelites (Betics, SE
 930 Spain). *Tectonophysics* 663, 122–139. <https://doi.org/10.1016/j.tecto.2015.08.036>
- 931 Booth-Rea, G., Ranero, C.R., Grevemeyer, I., 2018. The Alboran volcanic-arc modulated the Messinian faunal
 932 exchange and salinity crisis. *Scientific reports* 8, 13015. <https://doi.org/10.1038/s41598-018-31307-7>
- 933 Booth-Rea, G., Ranero, C.R., Martínez-Martínez, J.M., Grevemeyer, I., 2007. Crustal types and Tertiary tectonic
 934 evolution of the Alborán sea, western Mediterranean. *Geochemistry, Geophysics, Geosystems* 8, n/a-n/a.
 935 <https://doi.org/10.1029/2007gc001639>
- 936 Booth-Rea, G., Azañón, J.-M., Azor, A., García-Dueñas, V., 2004. Influence of strike-slip fault segmentation on
 937 drainage evolution and topography. A case study: the Palomares Fault Zone (southeastern Betics, Spain). *J*
 938 *Struct Geol* 26, 1615–1632. <https://doi.org/10.1016/j.jsg.2004.01.007>
- 939 Borque, M.J., Alzola, A.S., Martín-Rojas, I., Alfaro, P., Molina, S., Cintas, S.R., Caderot, G.R., Lacy, C., Avilés,
 940 M., Olmo, A.H., Tortosa, F.J.G., Estévez, A., Gil, A.J., 2019. How Much Nubia-Eurasia Convergence Is
 941 Accommodated by the NE End of the Eastern Betic Shear Zone (SE Spain)? Constraints From GPS Velocities.
 942 *Tectonics* 38, 271–1839. <https://doi.org/10.1029/2018tc004970>
- 943 Braga, J.C., Martín, J.M., Quesada, C., 2003. Patterns and average rates of late Neogene–Recent uplift of the Betic
 944 Cordillera, SE Spain. *Geomorphology* 50, 3–26. [https://doi.org/10.1016/s0169-555x\(02\)00205-2](https://doi.org/10.1016/s0169-555x(02)00205-2)
- 945 Carbonell, R., Sallares, V., Pous, J., Dañobeitia, J.J., Queralt, P., Ledo, J.J., Dueñas, V.G., 1998. A multidisciplinary
 946 geophysical study in the Betic chain (southern Iberia Peninsula). *Tectonophysics* 288, 137–152.
 947 [https://doi.org/10.1016/s0040-1951\(97\)00289-8](https://doi.org/10.1016/s0040-1951(97)00289-8)
- 948 Clark, S.J.P., Dempster, T.J., 2009. The record of tectonic denudation and erosion in an emerging orogen: an apatite
 949 fission-track study of the Sierra Nevada, southern Spain. *Journal of the Geological Society* 166, 87–100.
 950 <https://doi.org/10.1144/0016-76492008-041>

Deleted: Romain,

Deleted: Romain,

Deleted: <https://doi.org/10.1093/gji/ggu454>

Deleted: <https://doi.org/10.1029/2007gc001639>

955 Comas, M. C., J. J. Dañobeitia, J. Alvarez-Marón, and J. I. Soto (1995). Crustal reflections and structure in the
956 Alboran Basin. Preliminary results of the ESCI-Alboran survey, *Rev. Soc. Geol. Esp.*, 8(4), 529–542.
957 Comas, M.C., García-Dueñas, V., Jurado, M.J., 1992. Neogene tectonic evolution of the Alboran Sea from MCS
958 data. *Geo-mar Lett* 12, 157–164. <https://doi.org/10.1007/bf02084927>
959 Comas, M., and MARSIBAL 1-06 Scientific Party (2007). Preliminary results of Marsibal 1-06 cruise in the
960 Alboran and western Algero-Balearic basins. *Geophys. Res. Abst.*, 9, 10871.
961 Conand, C., Mouthereau, F., Ganne, J., Lin, A.T., Lahfid, A., Daudet, M., Mesalles, L., Giletycz, S., Bonzani, M.,
962 2020. Strain Partitioning and Exhumation in Oblique Taiwan Collision: Role of Rift Architecture and Plate
963 Kinematics. *Tectonics* 39, e2019TC005798. <https://doi.org/10.1029/2019tc005798>
964 ~~Crespo-Blanc, A., Comas, M., Balanva, J.C., 2016. Clues for a Tortonian reconstruction of the Gibraltar Arc:
965 Structural pattern, deformation diachronism and block rotations. *Tectonophysics* 683, 308–324.
966 <https://doi.org/10.1016/j.tecto.2016.05.045>~~
967 d’Acremont, E., Lafosse, M., Rabaute, A., Teurquety, G., Couto, D.D., Ercilla, G., Juan, C., Lepinay, B.M.,
968 Lafuerza, S., Galindo-Zaldivar, J., Estrada, F., Vazquez, J.T., Leroy, S., Poort, J., Ammar, A., Gorini, C., 2020.
969 Polyphase Tectonic Evolution of Fore-Arc Basin Related to STEP Fault as Revealed by Seismic Reflection Data
970 From the Alboran Sea (W-Mediterranean). *Tectonics* 39. <https://doi.org/10.1029/2019tc005885>
971 Dalziel, I.W.D., Lawver, L.A., Norton, I.O., Gahagan, L.M., 2013. The Scotia Arc: Genesis, Evolution, Global
972 Significance. *Annu Rev Earth Pl Sc* 41, 767–793. <https://doi.org/10.1146/annurev-earth-050212-124155>
973 Daudet, M., Mouthereau, F., Bricchau, S., Crespo-Blanc, A., Gautheron, C., Angrand, P., 2020. Tectono-
974 Stratigraphic and Thermal Evolution of the Western Betic Flysch: Implications for the Geodynamics of South
975 Iberian Margin and Alboran Domain. *Tectonics* 39. <https://doi.org/10.1029/2020tc006093>
976 Dewey, J.F., 1988. Extensional collapse of orogens. *Tectonics* 7, 1123–1139.
977 <https://doi.org/10.1029/tc007i006p01123>
978 Dewey, J.F., Helman, M.L., Knott, S.D., Turco, E., Hutton, D.H.W., 1989. Kinematics of the western
979 Mediterranean. Geological Society, London, Special Publications 45, 265–283.
980 <https://doi.org/10.1144/gsl.sp.1989.045.01.15>
981 Diaz, J., Gallart, J., Carbonell, R., 2016. Moho topography beneath the Iberian-Western Mediterranean region
982 mapped from controlled-source and natural seismicity surveys. *Tectonophysics* 692, 74–85.
983 <https://doi.org/10.1016/j.tecto.2016.08.023>
984 ~~Do Couto, D., Gumiaux, C., Augier, R., Lebret, N., Folcher, N., Jouannic, G., Jolivet, L., Suc, J., Gorini, C., 2014.
985 Tectonic inversion of an asymmetric graben: Insights from a combined field and gravity survey in the Sorbas
986 basin. *Tectonics* 33, 1360–1385. <https://doi.org/10.1002/2013tc003458>~~
987 Duggen, S., Hoernle, K., Bogaard, P. van den, Rupke, L., Morgan, J.P., 2003. Deep roots of the Messinian salinity
988 crisis. *Nature* 422, 602–606. <https://doi.org/10.1038/nature01553>
989 Duggen, S., Hoernle, K., Bogaard, P. van den, Harris, C., 2004. Magmatic evolution of the Alboran region: The role
990 of subduction in forming the western Mediterranean and causing the Messinian Salinity Crisis. *Earth Planet Sc*
991 *Lett* 218, 91–108. [https://doi.org/10.1016/s0012-821x\(03\)00632-0](https://doi.org/10.1016/s0012-821x(03)00632-0)
992 Duggen, S., Hoernle, K., Klugel, A., Geldmacher, J., Thirlwall, M., Hauff, F., Lowry, D., Oates, N., 2008.
993 Geochemical zonation of the Miocene Alboran Basin volcanism (westernmost Mediterranean): geodynamic
994 implications. *Contrib Mineral Petr* 156, 577. <https://doi.org/10.1007/s00410-008-0302-4>
995 Echeverria, A., Khazaradze, G., Asensio, E., Garate, J., Davila, J.M., Surinach, E., 2013. Crustal deformation in
996 eastern Betics from CuaTeNeo GPS network. *Tectonophysics* 608, 600–612.
997 <https://doi.org/10.1016/j.tecto.2013.08.020>
998 Ercilla, G., Galindo-Zaldivar, J., Estrada, F., Valencia, J., Juan, C., Casas, D., Alonso, B., Comas, M.C., Tendoro-
999 Salmeron, V., Casalbore, D., Azpiroz-Zabala, M., Barcenas, P., Ceramicola, S., Chiocci, F.L., Idarraga-Garcia,
1000 J., Lopez-Gonzalez, N., Mata, P., Palomino, D., Rodriguez-Garca, J.A., Teixeira, M., Nespereira, J., Vazquez,
1001 J.T., Yenes, M., 2022. Understanding the complex geomorphology of a deep sea area affected by continental
1002 tectonic indentation: The case of the Gulf of Vera (Western Mediterranean). *Geomorphology* 402, 108126.
1003 <https://doi.org/10.1016/j.geomorph.2022.108126>
1004 Faccenna, C., Becker, T.W., Auer, L., Billi, A., Boschi, L., Brun, J.P., Capitanio, F.A., Funicello, F., Horvath, F.,
1005 Jolivet, L., Piromallo, C., Royden, L., Rossetti, F., Serpelloni, E., 2014. Mantle dynamics in the Mediterranean.
1006 *Rev Geophys* 52, 283–332. <https://doi.org/10.1002/2013rg000444>
1007 Fortuin, A.R., Krijgsman, W., 2003. The Messinian of the Nijar Basin (SE Spain): sedimentation, depositional
1008 environments and paleogeographic evolution. *Sediment Geol* 160, 213–242. [https://doi.org/10.1016/s0037-0738\(02\)00377-9](https://doi.org/10.1016/s0037-0738(02)00377-9)

Deleted: Couto, D.

Moved down [2]: D., Gumiaux, C., Augier, R., Lebret, N., Folcher, N., Jouannic, G., Jolivet, L., Suc, J., Gorini, C., 2014. Tectonic inversion of an asymmetric graben: Insights from a combined field and gravity survey in the Sorbas basin. *Tectonics* 33, 1360–1385.

Deleted: <https://doi.org/10.1002/2013tc003458>

Formatted: French

Deleted: <https://doi.org/10.1016/j.tecto.2016.08.023>

Moved (insertion) [2]

Formatted: French

Deleted: <https://doi.org/10.1016/j.tecto.2013.08.020>

1019 Fossen, H., Teyssier, C., Whitney, D.L., 2013. Transtensional folding. *Journal of structural geology* 56, 89–102.
1020 <https://doi.org/http://dx.doi.org/10.1016/j.jsg.2013.09.004>

1021 Fossen, H., Tikoff, B., 1998. Extended models of transpression and transtension, and application to tectonic settings.
1022 Geological Society, London, Special Publications 135, 15–33. <https://doi.org/10.1144/gsl.sp.1998.135.01.02>

1023 Frasca, G., Gueydan, F., Brun, J.-P., Monié, P., 2016. Deformation mechanisms in a continental rift up to mantle
1024 exhumation. Field evidence from the western Betics, Spain. *Mar Petrol Geol* 76, 310–328.
1025 <https://doi.org/10.1016/j.marpetgeo.2016.04.020>

1026 Galindo-Zaldivar, J., Gonzalez-Lodeiro, F., Jabaloy, A., 2015. Progressive extensional shear structures in a
1027 detachment contact in the Western Sierra Nevada (Betic Cordilleras, Spain). *Geodin Acta* 3, 73–85.
1028 <https://doi.org/10.1080/09853111.1989.11105175>

1029 Galindo-Zaldivar, J., Gil, A.J., Borque, M.J., González-Lodeiro, F., Jabaloy, A., Marin-Lechado, C., Ruano, P.,
1030 Galdeano, C.S. de, 2003. Active faulting in the internal zones of the central Betic Cordilleras (SE, Spain). *J*
1031 *Geodyn* 36, 239–250. [https://doi.org/10.1016/s0264-3707\(03\)00049-8](https://doi.org/10.1016/s0264-3707(03)00049-8)

1032 Gallais, F., Graindorge, D., Gutscher, M.-A., Klaeschen, D., 2013. Propagation of a lithospheric tear fault (STEP)
1033 through the western boundary of the Calabrian accretionary wedge offshore eastern Sicily (Southern Italy).
1034 *Tectonophysics* 602, 141–152. <https://doi.org/10.1016/j.tecto.2012.12.026>

1035 ~~García-Castellanos, D., Villaseñor, A., 2012. Messinian salinity crisis regulated by competing tectonics and erosion
1036 at the Gibraltar arc. *Nature* 480, 359–363. <https://doi.org/10.1038/nature10651>~~

1037 García-Dueñas, V., Banda, E., Torné, M., Córdoba, D., Group, E.-B.W., 1994. A deep seismic reflection survey
1038 across the Betic Chain (southern Spain): first results. *Tectonophysics* 232, 77–89. [https://doi.org/10.1016/0040-1951\(94\)90077-9](https://doi.org/10.1016/0040-1951(94)90077-9)

1039 ~~1951(94)90077-9~~

1040 ~~Giaconia, F., Booth-Rea, G., Martínez-Martínez, J.M., Azañón, J.M., Pérez-Peña, J.V., Pérez-Romero, J., Villegas,
1041 I., 2012. Geomorphic evidence of active tectonics in the Sierra Alhamilla (eastern Betics, SE Spain).
1042 *Geomorphology* 145, 90–106. <https://doi.org/10.1016/j.geomorph.2011.12.043>~~

1043 ~~Giaconia, F., Booth-Rea, G., Martínez-Martínez, J.M., Azañón, J.M., Pérez-Romero, J., Villegas, I., 2013. Mountain
1044 front migration and drainage captures related to fault segment linkage and growth: The Polopos transpressive
1045 fault zone (southeastern Betics, SE Spain). *J Struct Geol* 46, 76–91. <https://doi.org/10.1016/j.jsg.2012.10.005>~~

1046 ~~Giaconia, F., Booth-Rea, G., Martínez-Martínez, J.M., Azañón, J.M., Storti, F., Artoni, A., 2014. Heterogeneous
1047 extension and the role of transfer faults in the development of the southeastern Betic basins (SE Spain).
1048 *Tectonics* 33, 2467–2489. <https://doi.org/10.1002/2014tc003681>~~

1049 Gómez-Pugnaire, M.T., Fernandez-Soler, J.M., 1987. High-pressure metamorphism in metabasites from the Betic
1050 Cordilleras (S.E. Spain) and its evolution during the Alpine orogeny. *Contrib Mineral Petr* 95, 231–244.
1051 <https://doi.org/10.1007/bf00381273>

1052 ~~Gómez de la Peña, L.G. de la, Grevemeyer, I., Kopp, H., Díaz, J., Gallart, J., Booth-Rea, G., Gràcia, E., Ranero,
1053 C.R., 2020a. The Lithospheric Structure of the Gibraltar Arc System From Wide-Angle Seismic Data. *J Geophys
1054 Res Solid Earth* 125. <https://doi.org/10.1029/2020jb019854>~~

1055 ~~Gómez de la Peña, L.G. de la, Ranero, C.R., Gràcia, E., 2018. The Crustal Domains of the Alboran Basin (Western
1056 Mediterranean). *Tectonics* 37, 3352–3377. <https://doi.org/10.1029/2017tc004946>~~

1057 ~~Gómez de la Peña, L.G. de la, Ranero, C.R., Gràcia, E., Booth-Rea, G., 2020b. The evolution of the westernmost
1058 Mediterranean basins. *Earth-sci Rev* 103445. <https://doi.org/10.1016/j.earscirev.2020.103445>~~

1059 Govers, R., Wortel, M.J.R., 2005. Lithosphere tearing at STEP faults: response to edges of subduction zones. *Earth
1060 Planet Sc Lett* 236, 505–523. <https://doi.org/10.1016/j.epsl.2005.03.022>

1061 Haq, B., Gorini, C., Baur, J., Moneron, J., & Rubino, J.-L. (2020). Deep Mediterranean's Messinian evaporite giant:
1062 How much salt? *Global and Planetary Change*, 184, 103052.
1063 doi:<https://doi.org/10.1016/j.gloplacha.2019.103052>

1064 Haughton, P.D.W., 2000. Evolving turbidite systems on a deforming basin floor, Tabernas, SE Spain.
1065 *Sedimentology* 47, 497–518. <https://doi.org/10.1046/j.1365-3091.2000.00293.x>

1066 Haughton, P.D.W., 1994. Deposits of deflected and ponded turbidity currents, Sorbas Basin, Southeast Spain. *J*
1067 *Sediment Res* 64, 233–246. <https://doi.org/10.1306/d4267d6b-2b26-11d7-8648000102c1865d>

1068 Heit, B., Mancilla, F. de L., Yuan, X., Morales, J., Stich, D., Martín, R., Molina-Aguilera, A., 2017. Tearing of the
1069 mantle lithosphere along the intermediate-depth seismicity zone beneath the Gibraltar Arc: The onset of
1070 lithospheric delamination. *Geophys Res Lett* 44, 4027–4035. <https://doi.org/10.1002/2017gl073358>

1071 Hinsbergen, D.J.J., Vissers, R.L.M., Spakman, W., 2014. Origin and consequences of western Mediterranean
1072 subduction, rollback, and slab segmentation. *Tectonics* 33, 393–419. <https://doi.org/10.1002/2013tc003349>

Deleted: <https://doi.org/10.1016/j.tecto.2012.12.026>

Deleted: [https://doi.org/10.1016/0040-1951\(94\)90077-9](https://doi.org/10.1016/0040-1951(94)90077-9)

Deleted: <https://doi.org/10.1016/j.jsg.2012.10.005>

Moved (insertion) [3]

Moved (insertion) [4]

Moved (insertion) [5]

1076 Hodgson, D.M., Haughton, P.D.W., 2004. Impact of syndepositional faulting on gravity current behaviour and deep-
1077 water stratigraphy: Tabernas-Sorbas Basin, SE Spain. *Geological Soc Lond Special Publ* 222, 135–158.
1078 <https://doi.org/10.1144/gsl.sp.2004.222.01.08>
1079 Jabaloy-Sánchez, A., Talavera, C., Rodríguez-Peces, M.J., Vázquez-Vilchez, M., Evans, N.J., 2021. U-Pb
1080 geochronology of detrital and igneous zircon grains from the Águilas Arc in the Internal Betics (SE Spain):
1081 Implications for Carboniferous-Permian paleogeography of Pangea. *Gondwana Res* 90, 135–158.
1082 <https://doi.org/10.1016/j.gr.2020.10.013>
1083 Janowski, M., Loget, N., Gautheron, C., Barbarand, J., Bellahsen, N., Driessche, J.V. den, Babault, J., Meyer, B.,
1084 2017. Neogene exhumation and relief evolution in the eastern Betics (SE Spain): Insights from the Sierra de
1085 Gador. *Terra Nova* 29, 91–97. <https://doi.org/10.1111/ter.12252>
1086 Johnson, C., Harbury, N., Hurford, A.J., 1997. The role of extension in the Miocene denudation of the Nevado-
1087 Filábride Complex, Betic Cordillera (SE Spain). *Tectonics* 16, 189–204. <https://doi.org/10.1029/96tc03289>
1088 Jolivet, L., Baudin, T., Calassou, S., Chevrot, S., Ford, M., Issautier, B., Lasseur, E., Masini, E., Manatschal, G.,
1089 Mouthereau, F., Thion, I., Vidal, O., 2021a. Geodynamic evolution of a wide plate boundary in the Western
1090 Mediterranean, near-field versus far-field interactions. *Bsgf - Earth Sci Bulletin* 192, 48.
1091 <https://doi.org/10.1051/bsgf/2021043>
1092 Jolivet, L., Faccenna, C., 2000. Mediterranean extension and the Africa-Eurasia collision. *Tectonics* 19, 1095–1106.
1093 <https://doi.org/10.1029/2000tc900018>
1094 Jolivet, L., Menant, A., Roche, V., Pourhiet, L.L., Maillard, A., Augier, R., Couto, D.D., Gorini, C., Thion, I.,
1095 Canva, A., 2021b. Transfer zones in Mediterranean back-arc regions and tear faults. *Bsgf - Earth Sci Bulletin*
1096 192, 11. <https://doi.org/10.1051/bsgf/2021006>
1097 Jourdon, A., Kergaravat, C., Duclaux, G., Huguen, C., 2021. Looking beyond kinematics: 3D thermo-mechanical
1098 modelling reveals the dynamics of transform margins. *Solid Earth* 12, 1211–1232. <https://doi.org/10.5194/se-12-1211-2021>
1099
1100 Juan, C., Ercilla, G., Javier Hernández-Molina, F., Estrada, F., Alonso, B., Casas, D., . . . Ammar, A. (2016).
1101 Seismic evidence of current-controlled sedimentation in the Alboran Sea during the Pliocene and Quaternary:
1102 Palaeoceanographic implications. *Marine Geology*, 378, 292-311.
1103 doi:<https://doi.org/10.1016/j.margeo.2016.01.006>
1104 Jurado, M.J., Comas, M.C., 1992. Well log interpretation and seismic character of the cenozoic sequence in the
1105 northern Alboran Sea. *Geo-Marine Letters* 12, 129–136.
1106 Kleverlaan, K., 1989. Neogene history of the Tabernas basin (SE Spain) and its Tortonian submarine fan
1107 development. *Geologie en Mijnbouw* 421–432.
1108 Kleverlaan, K., 1989. Three distinctive feeder-lobe systems within one time slice of the Tortonian Tabernas fan, SE
1109 Spain. *Sedimentology* 36, 25–45. <https://doi.org/10.1111/j.1365-3091.1989.tb00818.x>
1110 Kleverlaan, K., 1987. Gordo megabed: a possible seismite in a tortonian submarine fan, tabernas basin, province
1111 almeria, southeast spain. *Sediment Geol* 51, 165–180. [https://doi.org/10.1016/0037-0738\(87\)90047-9](https://doi.org/10.1016/0037-0738(87)90047-9)
1112 Koulali, A., Ouazar, D., Tahayt, A., King, R.W., Vernant, P., Reilinger, R.E., McClusky, S., Mourabit, T., Davila,
1113 J.M., Amraoui, N., 2011. New GPS constraints on active deformation along the Africa-Iberia plate boundary.
1114 *Earth Planet Sc Lett* 308, 211–217. <https://doi.org/10.1016/j.epsl.2011.05.048>
1115 Larouzière, F.D.D., Bolze, J., Bordet, P., Hernandez, J., Montecat, C., d'Estevou, P.O., 1988. The Betic segment of
1116 the lithospheric Trans-Alboran shear zone during the Late Miocene. *Tectonophysics* 152, 41–52.
1117 [https://doi.org/10.1016/0040-1951\(88\)90028-5](https://doi.org/10.1016/0040-1951(88)90028-5)
1118 Lonergan, L., White, N., 1997. Origin of the Betic-Rif mountain belt. *Tectonics* 16, 504–522.
1119 <https://doi.org/10.1029/96tc03937>
1120 Mancilla, F. de L., Booth-Rea, G., Stich, D., Pérez-Peña, J.V., Morales, J., Azañón, J.M., Martín, R., Giaconia, F.,
1121 2015a. Slab rupture and delamination under the Betics and Rif constrained from receiver functions.
1122 *Tectonophysics*. <https://doi.org/10.1016/j.tecto.2015.06.028>
1123 Mancilla, F. de L., Heit, B., Morales, J., Yuan, X., Stich, D., Molina-Aguilera, A., Azañón, J.M., Martín, R., 2018.
1124 A STEP fault in Central Betics, associated with lateral lithospheric tearing at the northern edge of the Gibraltar
1125 arc subduction system. *Earth Planet Sc Lett* 486, 32–40. <https://doi.org/10.1016/j.epsl.2018.01.008>
1126 Mancilla, F. de L., Stich, D., Morales, J., Martín, R., Diaz, J., Pazos, A., Córdoba, D., Pulgar, J.A., Ibarra, P.,
1127 Harnafi, M., Gonzalez-Lodeiro, F., 2015b. Crustal thickness and images of the lithospheric discontinuities in the
1128 Gibraltar arc and surrounding areas. *Geophysical Journal International* 203, 1804–1820.
1129 <https://doi.org/10.1093/gji/ggv390>
1130 Martín, J.M., Braga, J.C., Rivas, P., 1989. Coral successions in Upper Tortonian reefs in SE Spain. *Lethaia* 22, 271–
1131 286. <https://doi.org/10.1111/j.1502-3931.1989.tb01342.x>

Deleted: <https://doi.org/10.1144/gsl.sp.2004.222.01.08>

Deleted: BELLAHSEN

- 1134 Martín, J.M., Braga, J.C., 1994. Messinian events in the Sorbas Basin in southeastern Spain and their implications in
1135 the recent history of the Mediterranean. *Sediment Geol* 90, 257–268. <https://doi.org/10.1016/0037->
1136 0738(94)90042-6
- 1137 Martínez-García, P., Comas, M., Lonergan, L., Watts, A.B., 2017. From Extension to Shortening: Tectonic
1138 Inversion Distributed in Time and Space in the Alboran Sea, Western Mediterranean. *Tectonics* 36, 2777–2805.
1139 <https://doi.org/10.1002/2017tc004489>
- 1140 Martínez-García, P., Soto, J.I., Comas, M., 2011. Recent structures in the Alboran Ridge and Yusuf fault zones
1141 based on swath bathymetry and sub-bottom profiling: evidence of active tectonics. *Geo-mar Lett* 31, 19–36.
1142 <https://doi.org/10.1007/s00367-010-0212-0>
- 1143 Martínez-Martínez, J.M., Azañón, J.M., 1997. Mode of extensional tectonics in the southeastern Betics (SE Spain):
1144 Implications for the tectonic evolution of the peri-Alborán orogenic system. *Tectonics* 16, 205–225.
1145 <https://doi.org/10.1029/97tc00157>
- 1146 Martínez-Martínez, J.M., Booth-Rea, G., Azañón, J.M., Torcal, F., 2006. Active transfer fault zone linking a
1147 segmented extensional system (Betics, southern Spain): Insight into heterogeneous extension driven by edge
1148 delamination. *Tectonophysics* 422, 159–173. <https://doi.org/10.1016/j.tecto.2006.06.001>
- 1149 Martínez-Martínez, J.M., Soto, J.I., Balanyá, J.C., 2002. Orthogonal folding of extensional detachments: Structure
1150 and origin of the Sierra Nevada elongated dome (Betics, SE Spain). *Tectonics* 21, 3-1-3–20.
1151 <https://doi.org/10.1029/2001tc001283>
- 1152 Martínez-Martos, M., Galindo-Zaldívar, J., Martínez-Moreno, F.J., Calvo-Rayó, R., Galdeano, C.S. de, 2017.
1153 Superposition of tectonic structures leading elongated intramontane basin: the Alhambra basin (Internal Zones,
1154 Betic Cordillera). *Int J Earth Sci* 106, 2461–2471. <https://doi.org/10.1007/s00531-016-1442-9>
- 1155 Meighan, H.E., Brink, U. ten, Pulliam, J., 2013. Slab tears and intermediate-depth seismicity: slab tears and
1156 intermediate seismicity. *Geophys Res Lett* 40, 4244–4248. <https://doi.org/10.1002/grl.50830>
- 1157 Meijninger, B.M.L., Vissers, R.L.M., 2006. Miocene extensional basin development in the Betic Cordillera, SE
1158 Spain revealed through analysis of the Alhambra de Murcia and Crevillente Faults: Miocene extensional basin
1159 development in the Betic Cordillera. *Basin Res* 18, 547–571. <https://doi.org/10.1111/j.1365-2117.2006.00308.x>
- 1160 Montecat, C., D'Estevou, P.O., 1992. Geodynamics of the Eastern Betic late Neogene Basins. A Review. *Física de*
1161 *la Tierra* 57–75.
- 1162 Mora, M., 1993. Tectonic and sedimentary analysis of the Huerca-Overa region, South East Spain, Betic Cordillera.
1163 University of Oxford, 300 pp.
- 1164 [Moragues, L., Ruano, P., Azañón, J.M., Garrido, C.J., Hidas, K., Booth-Rea, G., 2021. Two Cenozoic Extensional](https://doi.org/10.1029/2021tc006868)
1165 [Phases in Mallorca and Their Bearing on the Geodynamic Evolution of the Western Mediterranean. *Tectonics*](https://doi.org/10.1029/2021tc006868)
1166 [40. <https://doi.org/10.1029/2021tc006868>.](https://doi.org/10.1029/2021tc006868)
- 1167 Mouthereau, F., Angrand, P., Jourdon, A., Ternois, S., Fillon, C., Calassou, S., Chevrot, S., Ford, M., Jolivet, L.,
1168 Manatschal, G., Masini, E., Thion, I., Vidal, O., Baudin, T., 2021. Cenozoic mountain building and topographic
1169 evolution in Western Europe: impact of billions of years of lithosphere evolution and plate kinematics. *Bsgf -*
1170 *Earth Sci Bulletin* 192, 56. <https://doi.org/10.1051/bsgf/2021040>
- 1171 Mouthereau, F., Filleaudeau, P., Vacherat, A., Pik, R., Lacombe, O., Fellin, M.G., Castellort, S., Christophoul, F.,
1172 Masini, E., 2014. Placing limits to shortening evolution in the Pyrenees: Role of margin architecture and
1173 implications for the Iberia/Europe convergence. *Tectonics* 33, 2283–2314. <https://doi.org/10.1002/2014tc003663>
- 1174 Neuharth, D., Brune, S., Glerum, A., Morley, C.K., Yuan, X., Braun, J., 2021. Flexural strike-slip basins. *Geology*.
1175 <https://doi.org/10.1130/g49351.1>
- 1176 Nocquet, J.-M., 2012. Present-day kinematics of the Mediterranean: A comprehensive overview of GPS results.
1177 *Tectonophysics* 579, 220–242. <https://doi.org/10.1016/j.tecto.2012.03.037>
- 1178 Okay, A.I., Tüysüz, O., Kaya, Ş., 2004. From transpression to transtension: changes in morphology and structure
1179 around a bend on the North Anatolian Fault in the Marmara region. *Tectonophysics* 391, 259–282.
1180 <https://doi.org/10.1016/j.tecto.2004.07.016>
- 1181 Palano, M., González, P.J., Fernández, J., 2015. The Diffuse Plate boundary of Nubia and Iberia in the Western
1182 Mediterranean: Crustal deformation evidence for viscous coupling and fragmented lithosphere. *Earth and*
1183 *Planetary Science Letters* 430, 439–447. <https://doi.org/10.1016/j.epsl.2015.08.040>
- 1184 Palano, M., González, P.J., Fernández, J., 2013. Strain and stress fields along the Gibraltar Orogenic Arc:
1185 Constraints on active geodynamics. *Gondwana Res* 23, 1071–1088. <https://doi.org/10.1016/j.gr.2012.05.021>
- 1186 Palomeras, I., Thurner, S., Levander, A., Liu, K., Villaseñor, A., Carbonell, R., Harnafi, M., 2014. Finite-frequency
1187 Rayleigh wave tomography of the western Mediterranean: Mapping its lithospheric structure. *Geochemistry,*
1188 *Geophysics, Geosystems* 15, 140–160. <https://doi.org/10.1002/2013gc004861>

Deleted: JoséM

1190 Pedrera, A., Galindo-Zaldívar, J., Galdeano, C.S. de, López-Garrido, Á.C., 2007. Fold and fault interactions during
1191 the development of an elongated narrow basin: The Almanzora Neogene-Quaternary Corridor (SE Betic
1192 Cordillera, Spain): FOLD AND FAULT INTERACTIONS. *Tectonics* 26, n/a-n/a.
1193 <https://doi.org/10.1029/2007tc002138>

1194 Pedrera, A., Galindo-Zaldívar, J., Ruiz-Constán, A., Duque, C., Marín-Lechado, C., Serrano, I., 2009. Recent large
1195 fold nucleation in the upper crust: Insight from gravity, magnetic, magnetotelluric and seismicity data (Sierra de
1196 Los Filabres-Sierra de Las Estancias, Internal Zones, Betic Cordillera). *Tectonophysics* 463, 145–160.
1197 <https://doi.org/10.1016/j.tecto.2008.09.037>

1198 Pedrera, A., Galindo-Zaldívar, J., Tello, A., Marín-Lechado, C., 2010. Intramontane basin development related to
1199 contractional and extensional structure interaction at the termination of a major sinistral fault: The Huércal-
1200 Overa Basin (Eastern Betic Cordillera). *J Geodyn* 49, 271–286. <https://doi.org/10.1016/j.jog.2010.01.008>

1201 Pickering, K.T., Hodgson, D.M., Platzman, E., Clark, J.D., Stephens, C., 2001. A New Type of Bedform Produced
1202 by Backfilling Processes in a Submarine Channel, Late Miocene, Tabernas-Sorbas Basin, SE Spain. *J Sediment*
1203 *Res* 71, 692–704. <https://doi.org/10.1306/2dc40960-0e47-11d7-8643000102c1865d>

1204 Pindell, J.L., Kennan, L., 2009. Tectonic evolution of the Gulf of Mexico, Caribbean and northern South America in
1205 the mantle reference frame: an update. *Geological Soc Lond Special Publ* 328, 1–55.
1206 <https://doi.org/10.1144/sp328.1>

1207 Platt, J.P., Behr, W.M., Johanesen, K., Williams, J.R., 2013. The Betic-Rif Arc and Its Orogenic Hinterland: A
1208 Review. *Annual Review of Earth and Planetary Sciences* 41, 313–357. <https://doi.org/10.1146/annurev-earth-050212-123951>

1210 Platt, J.P., Kelley, S.P., Carter, A., Orozco, M., 2005. Timing of tectonic events in the Alpujárride Complex, Betic
1211 Cordillera, southern Spain. *J Geol Soc London* 162, 451–462. <https://doi.org/10.1144/0016-764903-039>

1212 Platt, J.P., Anczkiewicz, R., Soto, J.-I., Kelley, S.P., Thirlwall, M., 2006. Early Miocene continental subduction and
1213 rapid exhumation in the western Mediterranean. *Geology* 34, 981–984. <https://doi.org/10.1130/g22801a.1>

1214 Platt, J.P., Vissers, R.L.M., 1989. Extensional collapse of thickened continental lithosphere: A working hypothesis
1215 for the Alboran Sea and Gibraltar arc. *Geology* 17, 540–543. [https://doi.org/10.1130/0091-7613\(1989\)017<0540:ecotcl>2.3.co;2](https://doi.org/10.1130/0091-7613(1989)017<0540:ecotcl>2.3.co;2)

1216 Platt, J.P., Whitehouse, M.J., 1999. Early Miocene high-temperature metamorphism and rapid exhumation in the
1217 Betic Cordillera (Spain): evidence from U–Pb zircon ages. *Earth and Planetary Science Letters* 171, 591–605.

1218 Platzman, E.S., 1992. Paleomagnetic rotations and the kinematics of the Gibraltar arc. *Geology* 20, 311–314.
1219 [https://doi.org/10.1130/0091-7613\(1992\)020<0311:prtko>2.3.co;2](https://doi.org/10.1130/0091-7613(1992)020<0311:prtko>2.3.co;2)

1220 Poisson, A., Guezou, J.C., Ozturk, A., Inan, S., Temiz, H., Gürsöy, H., Kavak, K.S., ÖZDEN, S., 1996. Tectonic
1221 Setting and Evolution of the Sivas Basin, Central Anatolia, Turkey. *International Geology Review* 38, 838–853.
1222 <https://doi.org/10.1080/00206819709465366>

1223 Poisson, A.M., Morel, J.L., Andrieux, J., Coulon, M., Wernli, R., Guernet, C., 1999. The origin and development of
1224 neogene basins in the SE Betic Cordillera (SE Spain): a case study of the Tabernas-Sorbas and Huercal Overa
1225 basins. *J Petrol Geol* 22, 97–114. <https://doi.org/10.1111/j.1747-5457.1999.tb00461.x>

1226 Pourhiet, L.L., Huet, B., May, D.A., Labrousse, L., Jolivet, L., 2012. Kinematic interpretation of the 3D shapes of
1227 metamorphic core complexes: 3D SHAPES OF MCCs. *Geochem Geophys Geosystems* 13.
1228 <https://doi.org/10.1029/2012gc004271>

1229 Pownall, J.M., Hall, R., Watkinson, I.M., 2013. Extreme extension across Seram and Ambon, eastern Indonesia:
1230 evidence for Banda slab rollback. *Solid Earth* 4, 277–314. <https://doi.org/10.5194/se-4-277-2013>

1231 Rat, J., Mouthereau, F., Bricchau, S., Crémades, A., Bernet, M., Balvay, M., Ganne, J., Lahfid, A., Gautheron, C.,
1232 2019. Tectonothermal Evolution of the Cameros Basin: Implications for Tectonics of North Iberia. *Tectonics* 38,
1233 440–469. <https://doi.org/10.1029/2018tc005294>

1234 Rat, J., Mouthereau, F., Bricchau, S., Vacherat, A., Fillon, C., Gautheron, C., 2022. Timing and distribution of
1235 exhumation in the Ebro basin reveal a plate-scale 10 Ma geodynamic event. *Global Planet Change* 103973.
1236 <https://doi.org/10.1016/j.gloplacha.2022.103973>

1237 Reicherter, K., Hübscher, C., 2006. Evidence for a seafloor rupture of the Carboneras Fault Zone (southern Spain):
1238 Relation to the 1522 Almería earthquake? *J Seismol* 11, 15–26. <https://doi.org/10.1007/s10950-006-9024-0>

1239 Reinhardt, L.J., Dempster, T.J., Shroder, J.F., Persano, C., 2007. Tectonic denudation and topographic development
1240 in the Spanish Sierra Nevada. *Tectonics* 26, n/a-n/a. <https://doi.org/10.1029/2006tc001954>

1241 Richards, J.P., 2009. Postsubduction porphyry Cu-Au and epithermal Au deposits: Products of remelting of
1242 subduction-modified lithosphere. *Geology* 37, 247–250. <https://doi.org/10.1130/g25451a.1>

1243

Moved up [3]: Peña, L.G. de la, Grevenmeyer, I., Kopp, H., Diaz, J., Gallart, J., Booth-Rea, G., Gràcia, E., Ranero, C.R., 2020a. The Lithospheric Structure of the Gibraltar Arc System From Wide-Angle Seismic Data. *J Geophys Res Solid Earth* 125. <https://doi.org/10.1029/2020jb019854>

Moved up [4]: Peña, L.G. de la, Ranero, C.R., Gràcia, E., Booth-Rea, G., 2020b. The evolution of the westernmost Mediterranean basins. *Earth-sci Rev* 103445. <https://doi.org/10.1029/2017tc004946>

Moved up [5]: Peña, L.G. de la, Ranero, C.R., Gràcia, E., Booth-Rea, G., 2020b. The evolution of the westernmost Mediterranean basins. *Earth-sci Rev* 103445. <https://doi.org/10.1016/j.earscirev.2020.103445>

Deleted: <https://doi.org/10.1144/0016-764903-039>

Deleted: THE ORIGIN AND DEVELOPMENT OF NEOGENE BASINS IN THE SE BETIC CORDILLERA (SE SPAIN): A CASE STUDY OF THE TABERNAS-SORBAS AND HUERCAL OVERA BASINS.

Deleted: <https://doi.org/10.1029/2006tc001954>

1263 Riding, R., Braga, J.C., Martín, J.M., Sánchez-Almazo, I.M., 1998. Mediterranean Messinian Salinity Crisis:
1264 constraints from a coeval marginal basin, Sorbas, southeastern Spain. *Mar Geol* 146, 1–20.
1265 [https://doi.org/10.1016/s0025-3227\(97\)00136-9](https://doi.org/10.1016/s0025-3227(97)00136-9)
1266 Rodríguez-Fernández, J., Azor, A., Azañón, J.M., 2012. Tectonics of Sedimentary Basins 461–479.
1267 <https://doi.org/10.1002/9781444347166.ch23>
1268 Romagny, A., Jolivet, L., Menant, A., Bessi re, E., Maillard, A., Canva, A., Gorini, C., Augier, R., 2020. Detailed
1269 tectonic reconstructions of the Western Mediterranean region for the last 35 Ma, insights on driving
1270 mechanisms. *Bsgf - Earth Sci Bulletin* 191, 37. <https://doi.org/10.1051/bsgf/2020040>
1271 Rosenbaum, G., Lister, G.S., Duboz, C., 2002. Relative motions of Africa, Iberia and Europe during Alpine
1272 orogeny. *Tectonophysics* 359, 117–129. [https://doi.org/10.1016/s0040-1951\(02\)00442-0](https://doi.org/10.1016/s0040-1951(02)00442-0)
1273 Sanz de Galdeano, C.S., Vera, J.A., 1992. Stratigraphic record and palaeogeographical context of the Neogene
1274 basins in the Betic Cordillera, Spain. *Basin Res* 4, 21–36. <https://doi.org/10.1111/j.1365-2117.1992.tb00040.x>
1275 Sanz de Galdeano, C.S.D., Rodr guez-Fernandez, J., Lopez-Garrido, A.C., 1985. A strike-slip fault corridor within
1276 the Alpujarras Mountains (Betic Cordilleras, Spain). *Geol Rundsch* 74, 641–655.
1277 <https://doi.org/10.1007/bf01821218>
1278 Sanz de Galdeano, C.S. de, Alfaro, P., 2004. Tectonic significance of the present relief of the Betic Cordillera.
1279 *Geomorphology* 63, 175–190. <https://doi.org/10.1016/j.geomorph.2004.04.002>
1280 Scotney, P., Burgess, R., Rutter, E.H., 2000. 40Ar/39Ar age of the Cabo de Gata volcanic series and displacements
1281 on the Carboneras fault zone, SE Spain. *J Geol Soc London* 157, 1003–1008.
1282 <https://doi.org/10.1144/jgs.157.5.1003>
1283 Sosson, M., Morrillon, A.-C., Bourgois, J., F raud, G., Poupeau, G., Saint-Marc, P., 1998. Late exhumation stages
1284 of the Alpujarride Complex (western Betic Cordilleras, Spain): new thermochronological and structural data on
1285 Los Reales and Ojen nappes. *Tectonophysics* 285, 253–273. [https://doi.org/10.1016/s0040-1951\(97\)00274-6](https://doi.org/10.1016/s0040-1951(97)00274-6)
1286 Spakman, W., Wortel, R., 2004. The TRANSMED Atlas. The Mediterranean Region from Crust to Mantle 31–52.
1287 https://doi.org/10.1007/978-3-642-18919-7_2
1288 Spakman, W., Chertova, M.V., Berg, A. van Hinsbergen, D.J.J., 2018. Puzzling features of western Mediterranean
1289 tectonics explained by slab dragging. *Nat Geosci* 11. <https://doi.org/10.1038/s41561-018-0066-z>
1290 Stich, D., Serpelloni, E., Mancilla, F. de L., Morales, J., 2006. Kinematics of the Iberia–Maghreb plate contact from
1291 seismic moment tensors and GPS observations. *Tectonophysics* 426, 295–317.
1292 <https://doi.org/10.1016/j.tecto.2006.08.004>
1293 Teyssier, C., Tikoff, B., 1998. Strike-slip partitioned transpression of the San Andreas fault system: a lithospheric-
1294 scale approach. *Geological Soc Lond Special Publ* 135, 143–158. <https://doi.org/10.1144/gsl.sp.1998.135.01.10>
1295 Vacherat, A., Mouthereau, F., Pik, R., Bellahsen, N., Gautheron, C., Bernet, M., Daudet, M., Balansa, J., Tibari, B.,
1296 Jamme, R.P., Radal, J., 2016. Rift-to-collision transition recorded by tectonothermal evolution of the northern
1297 Pyrenees. *Tectonics* 35, 907–933. <https://doi.org/10.1002/2015tc004016>
1298 van Hinsbergen, D.J.J., Vissers, R.L.M., Spakman, W., 2014. Origin and consequences of western Mediterranean
1299 subduction, rollback, and slab segmentation. *Tectonics* 33, 393–419. <https://doi.org/10.1002/2013tc003349>
1300 V zquez, M., Jabaloy, A., Barbero, L., Stuart, F.M., 2011. Deciphering tectonic- and erosion-driven exhumation of
1301 the Nevado-Fil bride Complex (Betic Cordillera, Southern Spain) by low temperature thermochronology:
1302 Deciphering tectonic- and erosion-driven exhumation. *Terra Nova* 23, 257–263. <https://doi.org/10.1111/j.1365-3121.2011.01007.x>
1303 Verg s, J., Fern ndez, M., 2012. Tethys–Atlantic interaction along the Iberia–Africa plate boundary: The Betic–Rif
1304 orogenic system. *Tectonophysics* 579, 144–172. <https://doi.org/10.1016/j.tecto.2012.08.032>
1305 Vernant, P., Fadil, A., Mourabit, T., Ouazar, D., Koulali, A., Davila, J.M., Garate, J., McClusky, S., Reilinger, R.,
1306 2010. Geodetic constraints on active tectonics of the Western Mediterranean: Implications for the kinematics and
1307 dynamics of the Nubia-Eurasia plate boundary zone. *J Geodyn* 49, 123–129.
1308 <https://doi.org/10.1016/j.jog.2009.10.007>
1309 Villase nor, A., Chevrot, S., Harnafi, M., Gallart, J., Pazos, A., Serrano, I., C rdoba, D., Pulgar, J.A., Ibarra, P.,
1310 2015. Subduction and volcanism in the Iberia–North Africa collision zone from tomographic images of the
1311 upper mantle. *Tectonophysics*. <https://doi.org/10.1016/j.tecto.2015.08.042>
1312 Waldner, M., Bellahsen, N., Mouthereau, F., Bernet, M., Pik, R., Rosenberg, C.L., Balvay, M., 2021. Central
1313 Pyrenees Mountain Building: Constraints From New LT Thermochronological Data From the Axial Zone.
1314 *Tectonics* 40. <https://doi.org/10.1029/2020tc006614>
1315 Weijermars, R., Roep, Th.B., Eeckhout, B.V. den, Postma, G., Kleverlaan, K., 1985. Uplift history of a Betic fold
1316 nappe inferred from Neogene-Quaternary sedimentation and tectonics (in the Sierra Alhamilla and Almeria,
1317 Sorbas and Tabernas Basins of the Betic Cordilleras, SE Spain). *Geologie en Mijnbouw* 397–411.

Deleted: [https://doi.org/10.1016/s0025-3227\(97\)00136-9](https://doi.org/10.1016/s0025-3227(97)00136-9)

Deleted: https://doi.org/10.1007/978-3-642-18919-7_2

Deleted: <https://doi.org/10.1002/2015tc004016>

1322 Zeck, H.P., Monié, P., Villa, I.M., Hansen, B.T., 1992. Very high rates of cooling and uplift in the Alpine belt of the
1323 Betic Cordilleras, southern Spain. *Geology* 20, 79. [https://doi.org/10.1130/0091-](https://doi.org/10.1130/0091-7613(1992)020<0079:vhroca>2.3.co;2)
1324 [7613\(1992\)020<0079:vhroca>2.3.co;2](https://doi.org/10.1130/0091-7613(1992)020<0079:vhroca>2.3.co;2)
1325

Page 29: [1] Deleted

Frederic Mouthereau

09/05/2023 16:42:00

Page 29: [2] Formatted

Frederic Mouthereau

09/05/2023 16:42:00

English (US)